GEOTECHNICAL ENGINEERING

LUNAR SOIL PROPERTIES AND SOIL MECHANICS

FLOW IN POROUS MEDIA UNDER RAREFIED GAS CONDITIONS

FINAL REPORT FOR RESEARCH PHASE:

FLUID CONDUCTIVITY OF LUNAR SURFACE MATERIALS

by

F.C.HURLBUT and C.R.JIH

PREPARED FOR NASA HEADQUARTERS, WASHINGTON D.C.

UNDER NASA GRANT NGR 05-003-406

MAY 1972

SPACE SCIENCES LABORATORY

SERIES 13 ISSUE 43

UNIVERSITY OF CALIFORNIA • BERKELEY

GEOTECHNICAL ENGINEERING

LUNAR SOIL PROPERTIES AND SOIL MECHANICS

FLOW IN POROUS MEDIA UNDER RAREFIED GAS CONDITIONS

FINAL REPORT FOR RESEARCH PHASE:

FLUID CONDUCTIVITY OF LUNAR SURFACE MATERIALS

by

F. C. Hurlbut and C. R. Jih

Prepared for NASA Headquarters, Washington D. C.

Under NASA Grant NGR 05-003-406

April 1972

Space Sciences Laboratory

UNIVERSITY OF CALIFORNIA, BERKELEY

PREFACE

This report was prepared under NASA Grant NGR 05-003-406, Lunar Soil Properties and Soil Mechanics, for the National Aeronautics and Space Administration. Technical liaison for this work is conducted by the Assistant Administrator for University Affairs.

James K. Mitchell, Professor of Civil Engineering, served as Principal Investigator for these studies; Franklin C. Hurlbut, Professor of Aeronautical Sciences, served as co-investigator; Dr. H. John Hovland, Assistant Research Engineer, served as project manager; and Mr. C. Robert Jih, Graduate Research Assistant, participated in and executed much of the research described in this report.

ABSTRACT AND SUMMARY

This report brings to a conclusion research on the fluid conductivity of lunar surface materials under this grant, and summarizes investigations conducted on such phenomena between 1969 and 1971.

Within the initial period preliminary investigations indicated that:

1. Gas flow in lunar surface materials would be of the continuum, transitional and free-molecular types with the latter types always occurring at sufficient distances from gas sources.
2. New theoretical studies were needed to extend the framework within which analysis of experimental flow data might proceed.
3. Experimental studies were required to provide the physical basis for additional conceptual development.

Results of the theoretical and experimental programs responding to the above may be summarized as follows:

1. Theoretical methods were developed by Raghuraman[10] for the analysis of transitional and free-molecular flows, and for analysis of lunar permeability probe data in general as described by Witherspoon and Katz (Mitchell et al[9]), Witherspoon and Willis[13], and Hurlbut et al.[5]
2. Experimental studies of rarefied flows under conditions of a large pressure gradient (described in the body of this report) have shown flows in the continuum regime to be responsible for the largest portion of the pressure drop between source and sink for one dimensional flow, provided the entrance Knudsen number is sufficiently small, i.e., $Kn < 10^{-2}$.

3. The concept of local similarity (see Ref. 13 and present report) leading to a "universal" nondimensional function of Knudsen number was shown in the experimental work to have approximate validity. By means of this universal function flows in all regimes may be described in terms of an area fraction and a single length parameter. However, slightly differing behaviors of the various samples in the free-molecular regimes were found, suggesting the desirability of an extension of the analysis to include two length parameters.
4. Synthetic porous media prepared from glass beads exhibited flow behavior similar in many regards to that of a natural sandstone. It is suggested that studies using artificial stones with known pore configurations will lead to new insight concerning the structure of natural materials.
5. The experimental method developed in this work involving the use of segmented specimens of large permeability has been shown to be fruitful in the context of these investigations.

CONTENTS

INTRODUCTION

An experimental investigation of one-dimensional gas flows through porous bead beds and sandstone was undertaken for flow Knudsen numbers in the range 10^{-3} to $\approx 10^{2}$ based upon characteristic pore diameters. It is the purpose of this final report to describe the experimental apparatus and procedures and then to report and discuss the results.

The motivation for this study derived initially from an early objective of the lunar soils program to discover and develop means for the determination of the permeability of lunar surface materials through measurements *in situ*[8]. It was anticipated that such measurements might be accomplished through the use of a portable probe which would introduce gas at a measured pressure and flow rate into the material and which would then make use of a sampling of pressures at nearby points.

In the lunar environment the gas pressures associated with the probe may be expected to vary from the inlet pressure to near vacuum. It follows that a transition from continuum flow to free molecular flow will necessarily occur somewhere within the material. From preliminary study it was concluded that the development of a successful lunar permeability probe would require a wider understanding of flows in porous materials under rarefied gas conditions. To be more precise, an understanding was needed of flows which suffer transition from the continuum to the Knudsen (also termed free-molecule) flow regimes when passing from one region of the sample to another. We may assume these regimes of flow to be well characterized by the value of the Knudsen number, Kn, which in this context is given by the ratio of the molecular mean free path to the pore diameter. Thus an understanding was required of flows in which the Knudsen number changes within the material from values much smaller than unity near the

probe source to values much greater than unity as the flow approaches the sink region some distance away.

Although there is a modest body of work in the literature, on rarefied flows through capillaries as for example in references 1, 2, 3, 4, 6 and 7, none is of value in displaying the details of transitions occurring under conditions of large gas density gradient. Experimenters for the most part have arranged entrance and exit conditions to be sufficiently alike to preclude a change in regime within the test body, and corresponding limitations in boundary condition have ordinarily been imposed in theoretical studies. The experimental work of Sreekanth [11] on short tube flows constitutes a modest exception, but the ratio of exit to entrance Knudsen numbers was only 26 at maximum and pressure distributions over the tube length were not measured.

Perhaps the most direct theoretical attack on the problem of transition flow with arbitrary pressure ratios was completed recently by Raghuraman[10] using both a discrete ordinate method and a moment method. The configuration was that of a two dimensional slot. Unfortunately, the pressure ratio was limited to ten by problems of convergence and computation time. Extension to a cylindrical geometry seemed possible but more difficult.

Another kind of approach, essentially one of fitting and interpolation, is exemplified by the work of Zhdanov[14] and more recently of Wakao[12]. Parametric formulas for capillary flow are produced which give the flow rate as a function of Knudsen number for all regimes. However, it is assumed that the pressure ratios are never large enough to cause a transition of flow within the capillary. Thus the background in the field of our investigation is not rich. The most promising theoretical and experimental studies deal not with flows in porous media but with slot and capillary flows.

The present experiment is designed quite straightforwardly to examine flows in which transition occurs within the test body and to perform tests on porous solids rather than upon straight capillaries. Since it was essential that transition occur over a substantial distance along the axis of flow to permit the physical resolution of details of the pressure distribution, it was recognized that a volumetrically large, low density flow would be required. Such flows can be established only in materials of very high permeability; hence our initial decision to fabricate high permeability specimens from aggregates of coarse granular materials.

Examination of the requirements relating to pressure measurements at points intermediate to the ends of the specimen led to the present sample design. The specimen consists of a series of cylindrical segments co-axially alligned within a chamber which provides a gas seal along the perimeter of each segment. The planar interfaces are separated by small settling volumes, and pressure taps connect each of these volumes to the pressure metering system. Flow is axial and one-dimensional. A schematic of the geometry is shown in Figure 1 and more details of apparatus and sample construction are given at a later point in this report.

THEORY

It is our purpose in this section to develop generalized expressions which permit the display of certain features of flow behavior and of certain useful parameters as functions of Knudsen number. It is an assumption of this development that we may scale all phenomena in terms of Knudsen number based upon a single length parameter. The utility of this assumption is itself among the questions to be examined. The work follows very closely that already reported in an earlier project report by the present group[13].

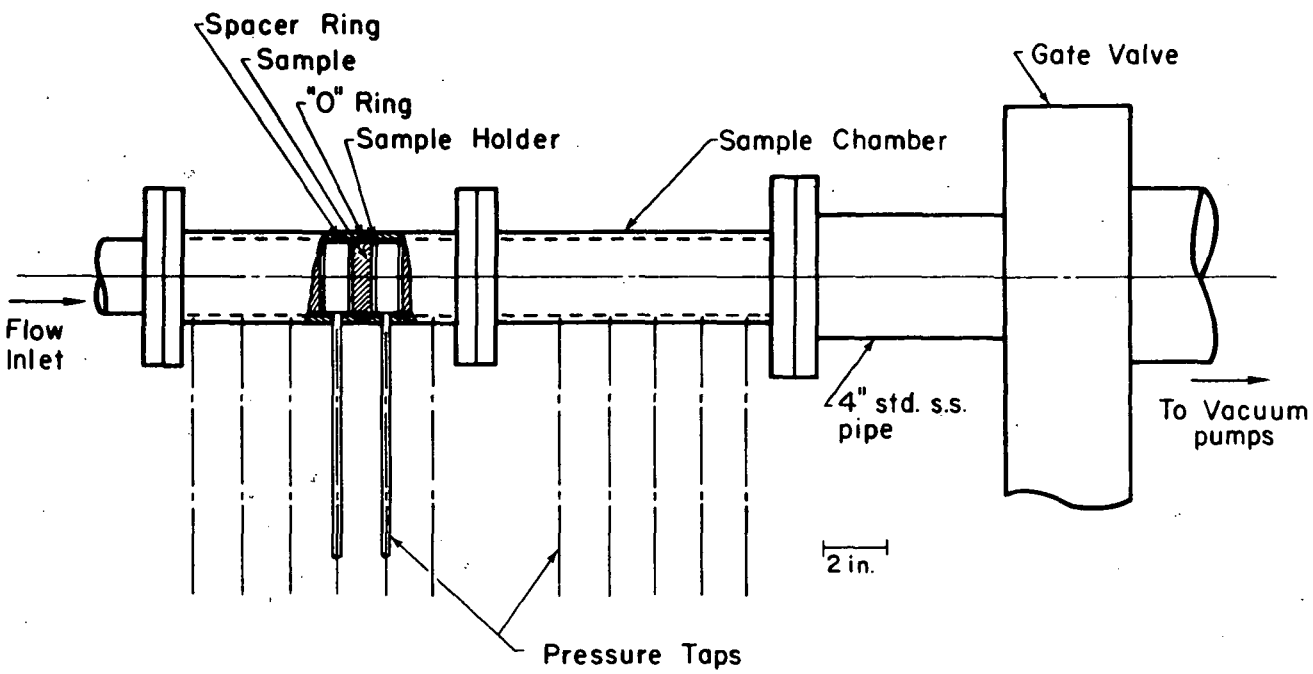

FIG. 1 SAMPLE CHAMBER SCHEMATIC (PARTIALLY SECTIONED)

Flows in porous media whether of liquids or gases are characteristically associated with low Reynolds numbers, the Reynolds number being based upon average flow speed and viscosity and upon the average pore size of the material. An expression which relates the mean flow speed, $\overline{V}$, to the gradient of pressure, ∇p, may be written from Darcy's law for one-dimensional flow as

$$\overline{V} = - c \nabla p \tag{1}$$

in which c is a dimensional constant. For incompressible continuum flow

$$c \equiv \frac{k}{\mu} \tag{2}$$

where k is the permeability with dimensions of length squared and μ is the absolute viscosity. In general, however, c will be a function of the pressure as well as the viscosity and also of the appropriate pore dimensions which characterize the particular system.

We now define a generalized coefficient, $\tilde{c}(p)$, such that

$$\tilde{c}(p) \equiv \frac{\mu}{L^2} c(p) \tag{3}$$

from which one may see that $\tilde{c}(p)$ is a dimensionless function of local pressure or Knudsen number only. Knudsen number and pressure are inversely proportional in this context. L^2 has dimensions of area and can be thought of as a generalized permeability, applicable in all flow regimes. We also assume steady isothermal flow in a porous medium which is homogeneous and isotropic. We assume that the steady condition of flow once established is independent of the initial state of pressure in the medium. These are the basic local similarity assumptions. We confine our attention to the one-dimensional case but recognize that the extension to more general cases can easily be made (see Ref. 12).

In addition we define, F(Kn), a function of Knudsen number, as

$$F(kn) \equiv \frac{1}{\tilde{c}(p)} \quad . \tag{4}$$

Thus the permeability k is given by the expression

$$k = \frac{L^2}{F(Kn)} \tag{5}$$

The Knudsen number is related to the viscosity and pressure through the expression

$$Kn = \frac{\lambda}{L} = \frac{2\mu\ RT}{L\ \bar{v}\ p} \tag{6}$$

in which $\bar{v}$ is the mean molecular speed, equal to $[8RT/\pi]^{1/2}$, R is the gas constant and λ is the molecular mean-free-path. In the present report the Knudsen number is calculated on the basis of L = 2a where a is the mean pore radius.

In accordance with the foregoing assumptions and definitions we write for the mass flow rate, Q,

$$Q = -\frac{L^2}{F(Kn)} \frac{fA}{\mu} \frac{p}{RT} \frac{dp}{dx} = \rho o\ \dot{\nabla} o \tag{7}$$

In the above f is an area fraction equal to the total pore area divided by the total cross sectional area, A is the cross sectional area of the sample, ρo is the upstream density and $\dot{\nabla} o$ is the upstream volumetric flow rate. From (7) we obtain

$$F(Kn) = \frac{fA}{\Delta x} \quad \frac{L^2}{2\mu} \quad \frac{\Delta p^2}{po\dot{\nabla} o} \tag{8}$$

in which finite differences have been introduced to reflect the physical nature of the experiment.

The function F(Kn) is a "universal" function based upon the local similarity concept. The utility of F(Kn) in the correlation of results obtained for the various regimes of flow will presently be examined.

Since F(Kn) is a function of pressure only we may also write from Eq. 7

$$\int_{x_1}^{x_2} po\ \dot{\nabla}o\ dx = \int_{p_2}^{p_1} \frac{fL^2A}{\mu}\ \frac{pdp}{F(Kn)} \tag{9}$$

Integration of the term on the left yields $po\ \dot{\nabla}o\ \ell_{1,2}$ which is equal to an integral function of pressure only taken between the limits $p_1 \equiv px_1$ and px_2. In examining the significance of Eq. 9 we find it useful to consider the following schematic of flow through the sample.

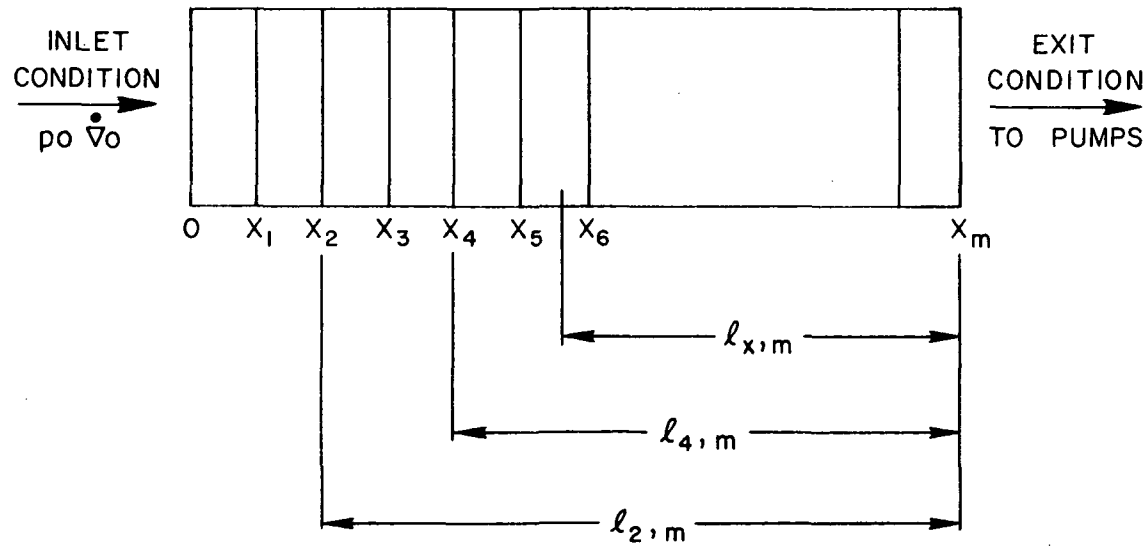

Pressures are measured at x_1, x_2, x_3, etc. to yield a particular distribution p_1, p_2 etc. for a particular setting of the quantity $po\ \dot{\nabla}o$. By changing the setting of the flow control valve we could, for example, arrange that the pressure which had been observed at x_4 would now be

measured at x_2 and we would now find a new distribution of pressures over the length of the sample. If the transition zone were formerly in the region ℓ_4, n it would now occur within the region ℓ_2, n and would be of similar configuration but somewhat more extended along the axis of flow, assuming of course that the down stream condition remained essentially unchanged. A further reduction in flow would result in a further extension of the transition region.

The foregoing considerations lead to a technique for scaling pressure related data obtained for several variations of inlet condition. These variations are introduced as a part of the experimental procedure to produce a scaling in length of the transition process. Accordingly we first pick a reference flow condition $(po\ \dot{\nabla}o)o$ such that all regimes are present in the sample. If now in some other more rarefied condition of flow with initial conditions $(po\ \dot{\nabla}o)_1$ we have observed a particular pressure at x_2, we scale from Eq. 9 to predict that it would have been observed at location x under the reference condition. Thus we may write

$$\ell_{x,n} = \frac{\ell_{2,n}\ (po\dot{\nabla}o)_1}{(po\dot{\nabla}o)o} \tag{10}$$

The length $\ell_{x,n}$ is a "reduced length". Similarly one may find reduced lengths for any other measured pressure in corresponding terms. Applications of the concept of reduced lengths in the reduction of data will be made at a later point in the report.

An interesting question, and one which is of importance from the design viewpoint concerns the identification of the flow regime which may be dominant during probe operation. In an earlier report the concept of the "sudden freeze" model was used to estimate the proportionality between the continuum and free-molecule regimes. Here we apply this

concept in the one-dimensional case.

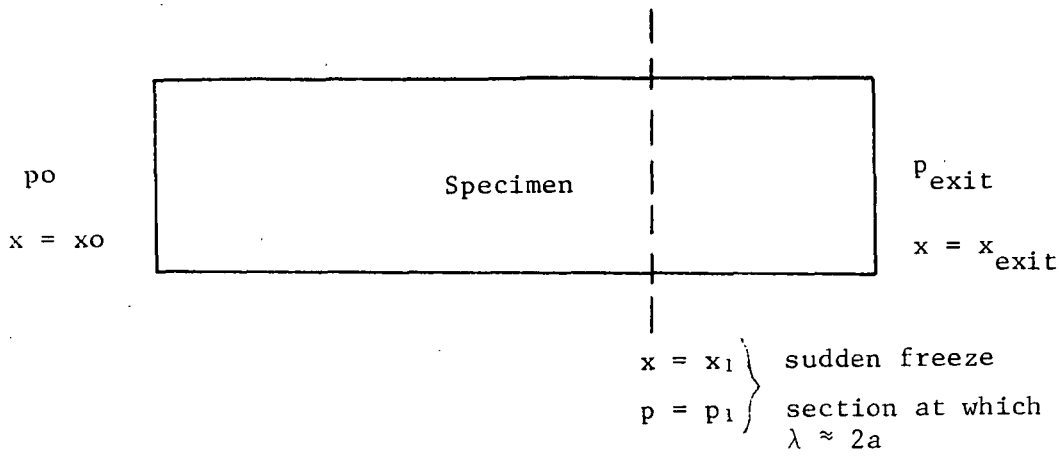

Darcy's Law for the continuum regime gives the mass flow, Q, as follows:

$$Q = - \frac{fAkp}{\mu RT} \frac{dp}{dx} \quad .$$

We integrate to the freeze section x_1 and obtain

$$Q = \frac{fkA}{2\mu RT} \frac{(po^2 - p_1^2)}{(x_1 - x_o)} \quad . \tag{11}$$

For the free molecular regime, Q is given by the expression

$$Q = - \frac{8}{3\pi} fA \frac{2a}{\bar{v}} \frac{dp}{dx}$$

which we integrate from x_1 to x exit to obtain

$$Q = \frac{8}{3\pi} fA \frac{2a}{\bar{v}} \frac{(p_1 - p_{exit})}{(x_{exit} - x_1)} \tag{12}$$

From Equations (11) and (12), letting p exit $\rightarrow$ 0 and assuming po $\approx$ p_1 we find

$$\frac{x_{exit} - x_1}{x_1 - x_o} \approx \frac{\lambda o^2}{k} \tag{13}$$

in which we have substituted for p_1; $p_1 = \frac{2\mu RT}{\bar{v}2a}$, 2a being equal to the mean free path λ_1 at this point. If the permeability k at the continuum end is now set equal to a constant of order one multiplied by $4a^2$, the ratio of free-molecule flow length to continuum flow length is approximately equal to the square of the upstream Knudsen number. Thus

$$\frac{x_{exit} - x_1}{x_1 - x_o} \approx (Kn_o)^2 \tag{14}$$

The applicability of this model remains to be examined in light of the experimental results.

EXPERIMENTAL

APPARATUS

The low pressure permeability apparatus is connected with the large vacuum pumping system of the UC Rarefied Gas wind tunnel through a port and gate valve. The speed of the pumps and connecting manifold is more than adequate to maintain the exit pressure at the downstream end of the specimen to values of the order on one micron Hg. A schematic of the apparatus appears in Figure 2 and a photograph is shown in Figure 3. The specimen test section, flow control apparatus and pressure measuring system are described in the following paragraphs.

1) Gas Source. Bottled dry nitrogen gas is supplied through pressure regulators and precision needle valve.

2) Flow metering system. A set of laboratory flow raters (Fisher Porter Model 10A-1017A-LK) was installed in a suitable manifold. These meters permitted flow rate measurements over the range 600 to 5×10^{-3} cm^3/sec at standard conditions. At the lowest flow rates, that is in the

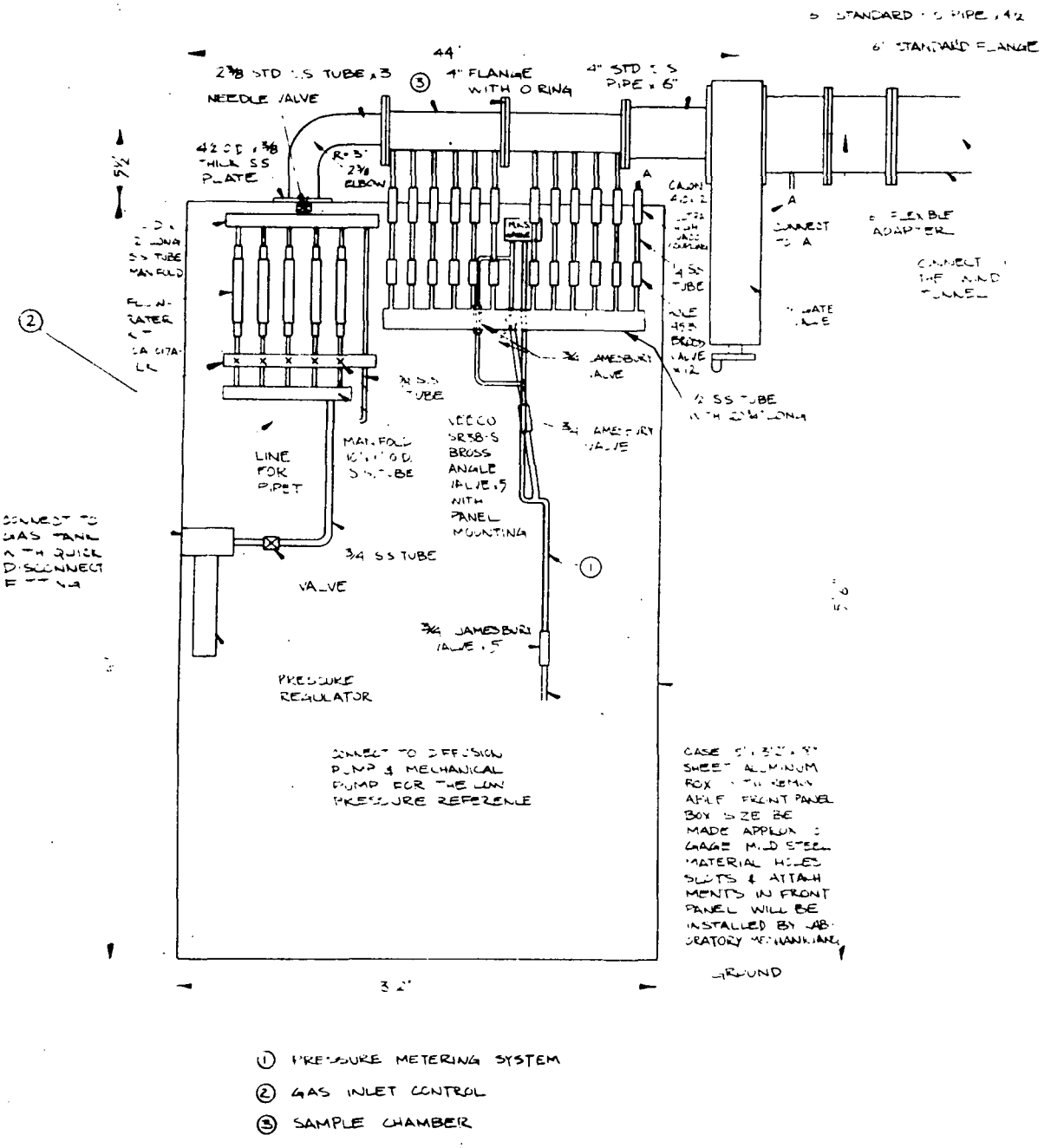

① PRESSURE METERING SYSTEM

② GAS INLET CONTROL

③ SAMPLE CHAMBER

Fig. 2. System assembly.

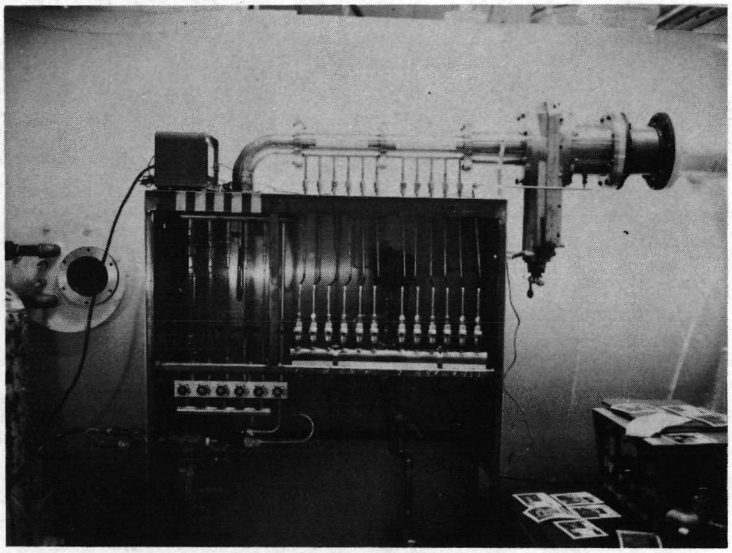

Fig. 3. View of the permeability apparatus

range 10^{-2} to 10^{-3} cm^3/sec, the well known pipette method was used. In this method the rate of travel of a soap film was measured.

3) Test Section. The test section is constructed of two demountable sections of stainless steel tubing with appropriate end flanges. Each section can contain up to five specimen segments and the necessary spacers. The specimen sections consist of a plexiglass outer ring 2 3/4" OD by 1" in length within which is cemented the sample itself. "O" rings provide the seal between the peripheral surface of the specimens and the inner wall of the chamber. At each mid-position of the space between samples there is a wall pressure tap. Each tap is connected to a single manifold through a toggle valve. Thus each intermediate region can be connected as required to the pressure manifold which in turn is connected to the transducer of the differential pressure gauge. Appropriate shut-off valves are incorporated.

4) Differential pressure gauge. The basic instrument is a differential pressure gauge of the diaphragm type manufactured by MKS Instruments Inc. (MKS Baratron, Type 77M-XR, 30 Torr to 0.01 Torr full scale). The manufacturer has provided a calibration chart which shows the accuracy to be within .3% on the lower range and .002% on the high range. The reproducibility is claimed to be better than 0.02% of full range on each scale. A mechanical and diffusion pumped vacuum system is attached to the reference leg of the metering system.

SAMPLE PREPARATION AND CHARACTERIZATION

In the initial period of this work it was determined that cast cement and sand samples were insufficiently permeable to permit effective testing at low gas densities. Flow rates were too small to be easily

measured and the response time of the gauging system was too large. After a little experimentation we found it possible to make suitable samples by sintering glass beads in a ring-shaped form of graphite. We also found that a grade of Boise sandstone was sufficiently permeable for our tests. Accordingly samples used in experimental program were of three types, 3 mm diameter glass beads, 4 mm diameter glass beads and natural sandstone.

In preparation of the sintered samples, beads of a particular size were placed in the graphite ring to a standard depth and then covered by a weight. The assemblage was shaken to achieve closer packing and then placed in an electric oven. The oven was slowly heated to 890-895°C, held at that temperature for 40 minutes and allowed to cool. Several samples were sintered at one time to insure a uniform history of preparation. A selection was then made of the eight or nine samples showing the most nearly equal permeability under atmospheric pressure conditions. Some shrinkage was observed to occur, being somewhat greater for the samples constructed of 4 mm diameter beads than for those constructed of 3 mm beads. The resultant pore configuration in the later case resembled more closely that for ideal close packed spheres. Photographs showing characteristic packing patterns in these samples are shown in Figures 4 and 5.

The sandstone specimens were cut from the natural Boise sandstone material to fit the specimen holding rings. Photographs of surface and pore configuration in this material are shown in Figure 6.

All specimens were cemented into ring holders using an epoxy cement which retained the samples and prevented gas from flowing between the sample edge and the ring holder.

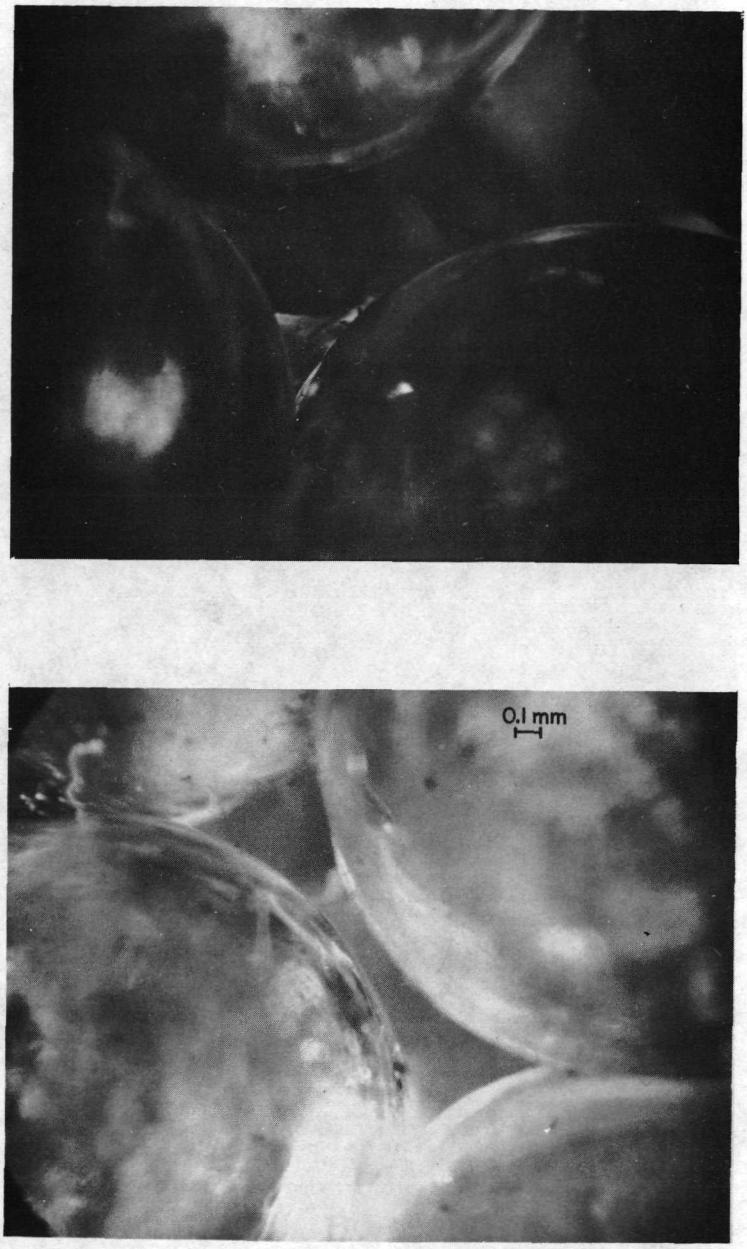

Fig. 4. 3 mm Sintered glass beads specimen

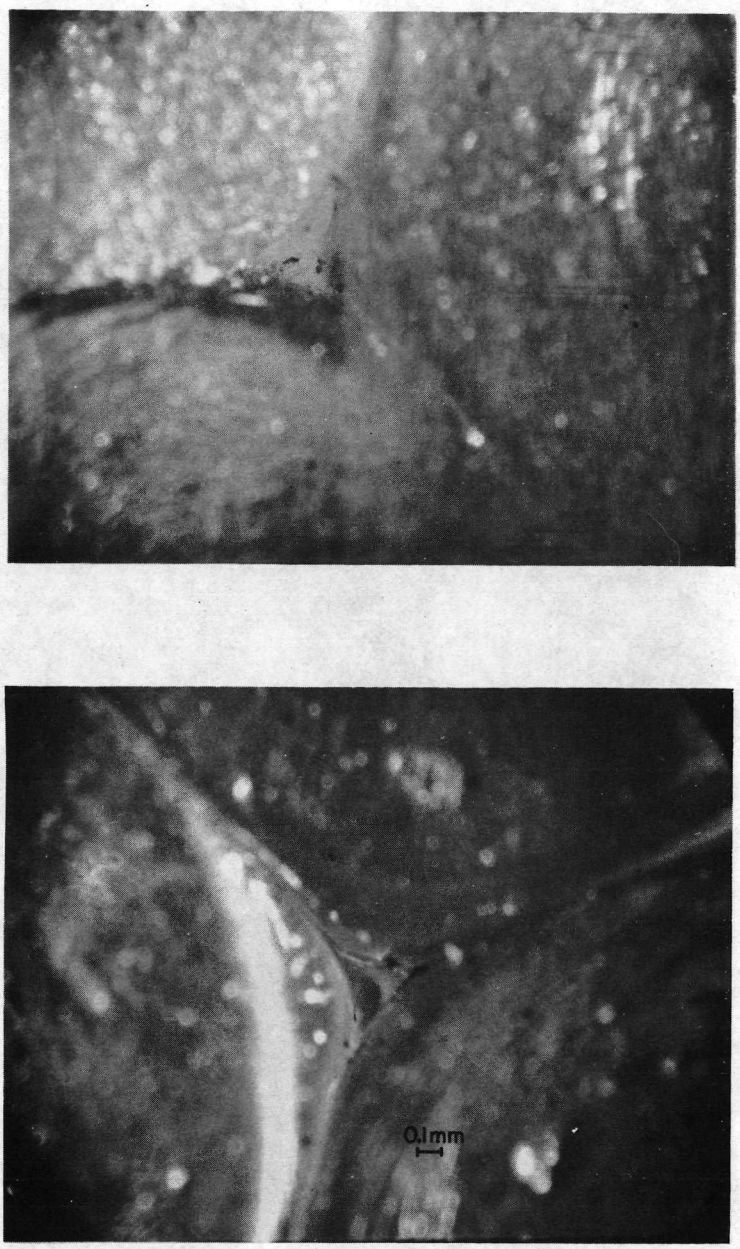

Fig. 5. 4 mm Sintered glass beads specimen

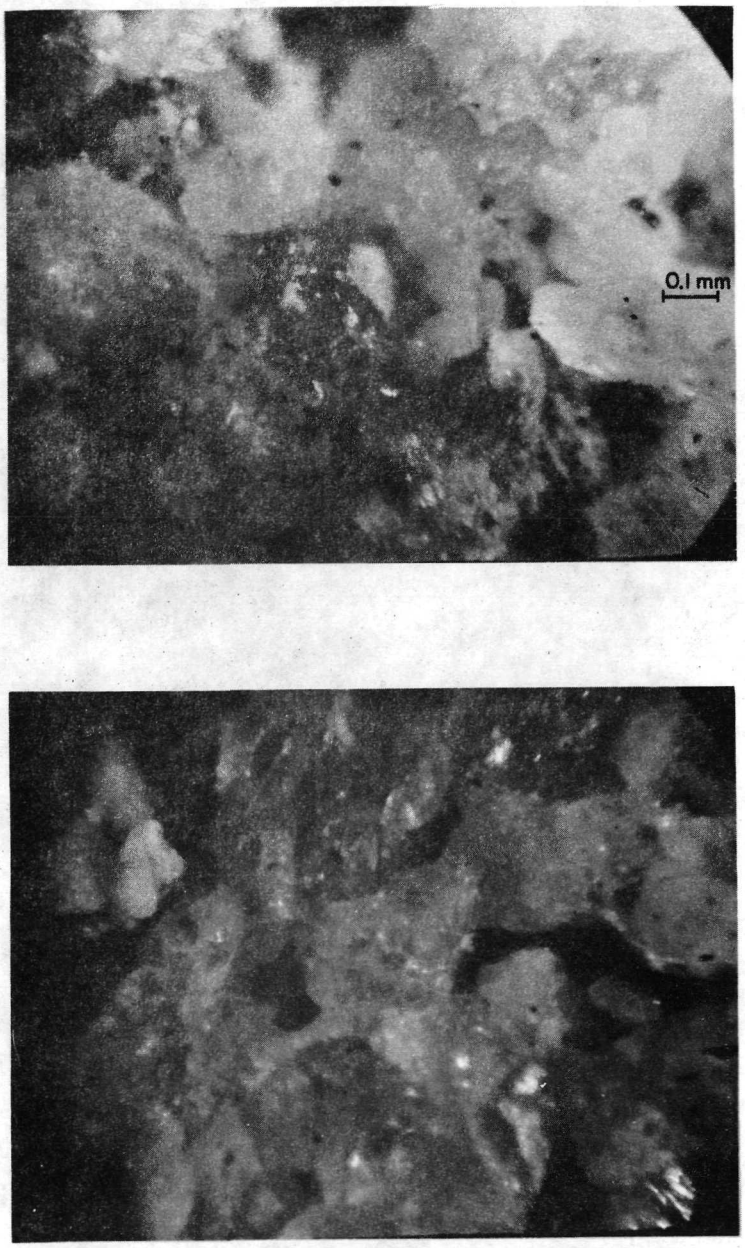

Fig. 6. Sand stone specimen

The porosity of the samples was measured by the gas expansion method. The pore size was measured by the capillary pressure distribution method and checked by measurements on the micro photographs. Results of these measurements are given in Table I.

Table I

Sample Characteristics

	3 mm Sintered Glass Beads	4 mm Sintered Glass Beads	Boise Sand Stone
Effective area fraction f	26.0%	5.74%	29.0%
Averaged pore size radius a (cm)	1.88×10^{-2}	1.23×10^{-2}	3.46×10^{-3}
Sample disk diameter (in)	1.960	1.991	1.991
Cross-sectional Area A (cm^2)	19.5	20.1	20.1
Thickness Δx (cm)	1.61	1.49	1.62
$\frac{fA}{\Delta x}$ (cm)	3.15	0.775	3.60

In the foregoing we have assumed the effective area fraction to be the same as the porosity. For the sandstone samples the pore is assumed to be circular. The pore shape in the case of the glass beads is more likely to be that of an equilateral triangle. We assume the characteristic length to be the hydraulic diameter which in this case is the diameter of the inscribed circle.

PROCEDURE

The specimens were set into the test chamber and allowed to degass under vacuum conditions. After the pressure had become stabilized and uniform throughout, nitrogen was introduced to the sample and allowed to flow for some time. Thereafter the sample was again evacuated. This process was repeated twice in order to insure that the gas flowing was indeed primarily that intended. Following this procedure the initial flow was established and pressure measurements obtained. The flow rate was readjusted repeatedly to expand the scale of transition according to the prescription outlined in the section on theory.

RESULTS AND DISCUSSION

All observations of pressure and flow rate together with computed values of permeability, Knudsen number and other quantities of significance are given in Tables II, III and IV. The samples were numbered in manufacture for identification and introduced in arbitrary order into the test sections. As is evident, the columns of data are ordered according to the physical arrangement of samples and not their numerical designators.

Calculated values of the quantity $\frac{fA}{\Delta x}\frac{\Delta p^2}{po\,\bar{\nabla}o}$ are plotted as functions of Kn in Figures 7, 8 and 9 for the three sets of samples. For comparison the interpolation formula due to Wakao was used to obtain predicted values over the same range of Knudsen numbers. Wakao's equation may be written (see Ref. 12) as

$$\left(\frac{k}{2\mu}\right)^{-1} = \frac{fA}{\Delta x}\frac{\Delta p}{po\bar{\nabla}o} = \frac{2p}{\left[\frac{DkA}{1+\frac{2a}{\lambda}} + \frac{DkA\,\frac{\pi}{4}\,\frac{2a}{\lambda}}{1+\frac{2a}{\lambda}} + \frac{\frac{pa^2}{8\mu}}{1+\frac{\lambda}{2a}}\right]} \quad . \qquad (15)$$

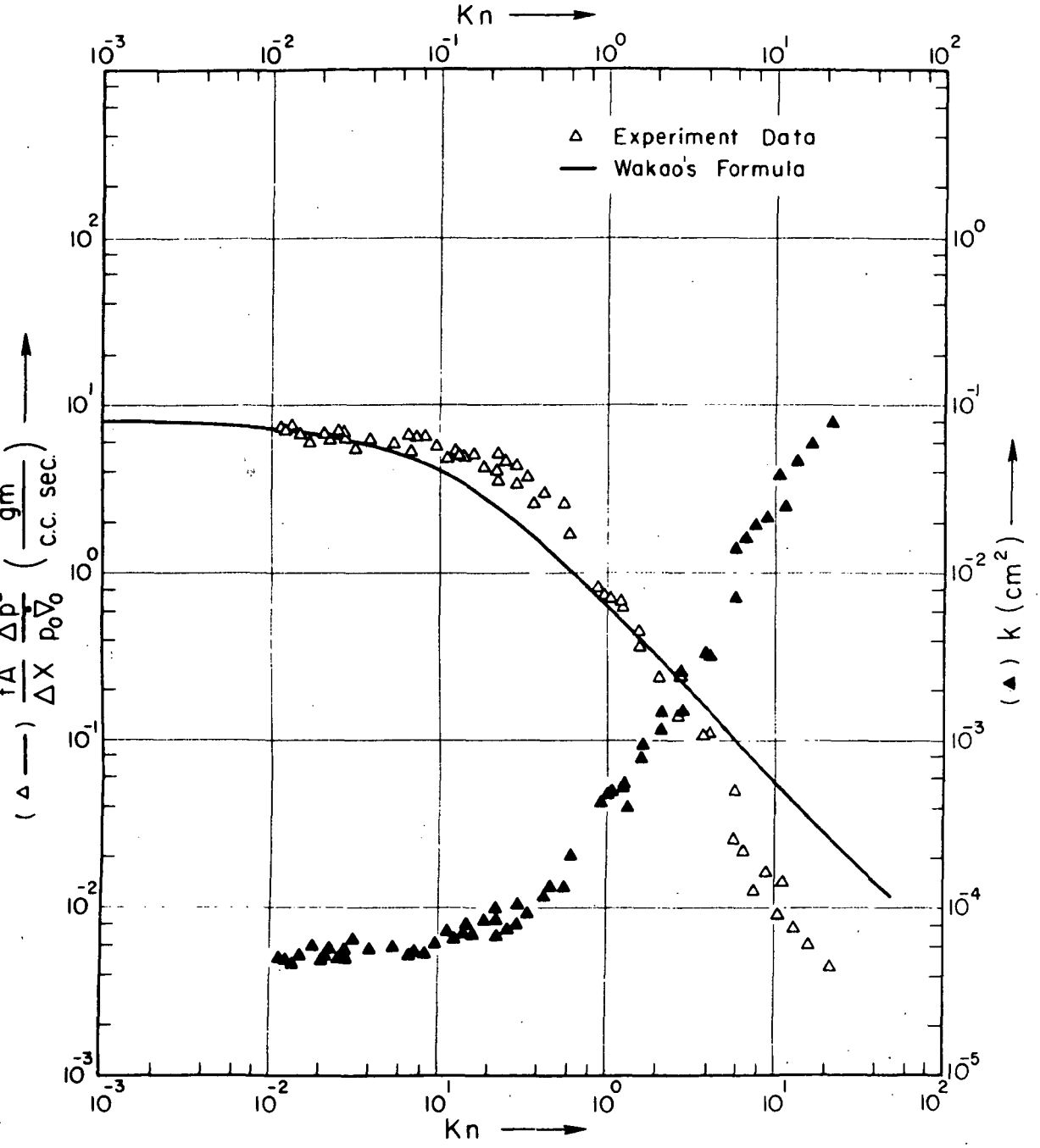

FIG. 7 $\frac{fA}{\Delta X}\frac{\Delta p^2}{p_0 \nabla_0}\left(\frac{gm}{c.c.\ sec.}\right)$ AND PERMEABILITY, k, VS Kn FOR 3mm SINTERED GLASS BEAD SPECIMEN

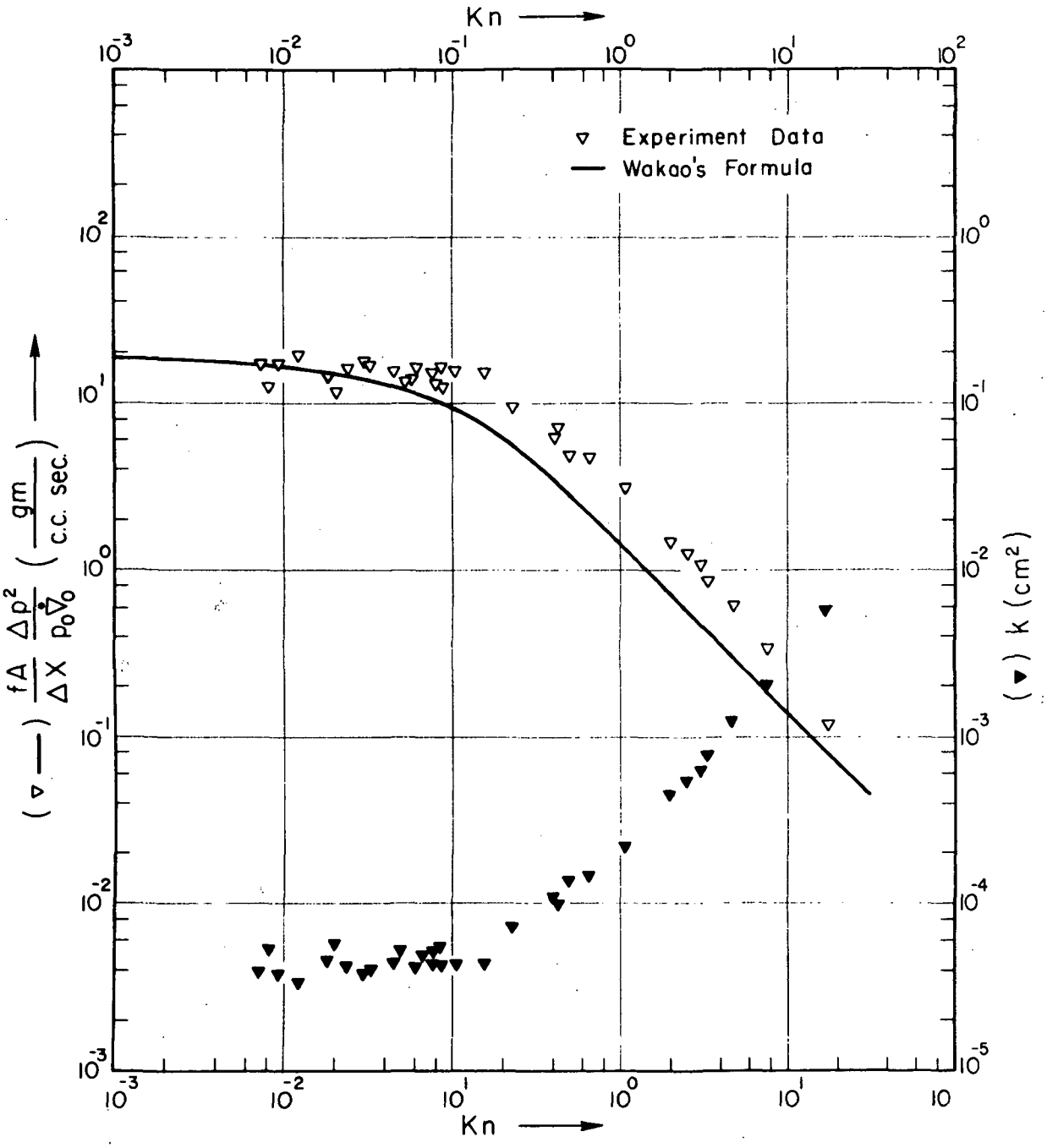

FIG. 8 $\frac{fA}{\Delta X}\frac{\Delta p^2}{p_0 \nabla_0}\left(\frac{gm}{c.c.\ sec.}\right)$ AND PERMEABILITY, k, VS Kn FOR 4mm SINTERED GLASS BEAD SPECIMEN

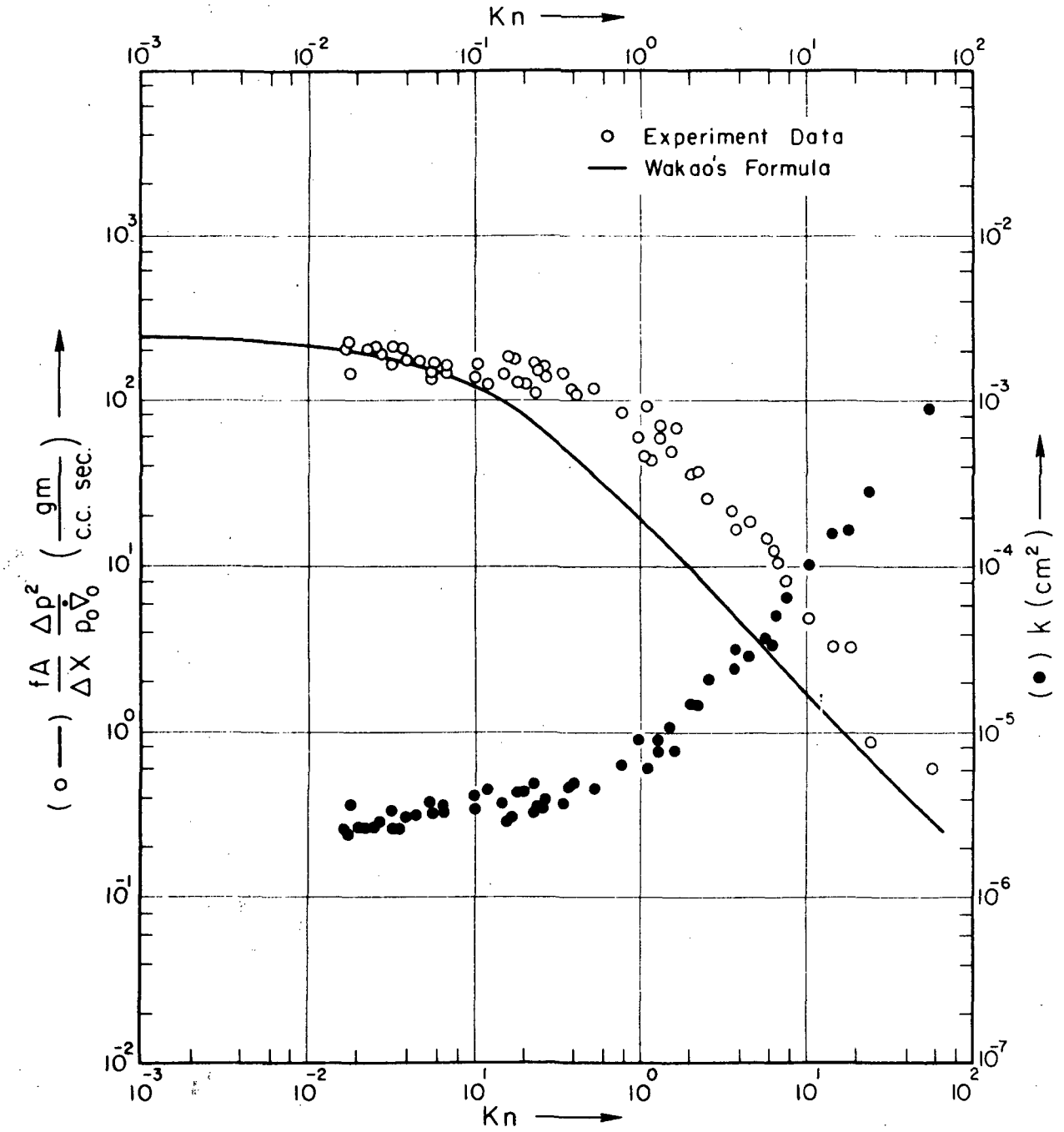

FIG. 9 $\frac{fA}{\Delta X}\frac{\Delta p^2}{p_o \dot{\nabla}_o}\left(\frac{gm}{c.c.\ sec.}\right)$ AND PERMEABILITY, k, VS Kn FOR SAND STONE SPECIMEN

If we substitute for Kn from $Kn = \frac{2\mu RT}{2a(\bar{v})} \frac{1}{p}$ we may rewrite the above as

$$\left(\frac{k}{2\mu}\right)^{-1} = \frac{\frac{2\mu RT}{a\bar{v}} (1 + Kn)}{\left[\frac{aRT}{8\bar{v}} + \frac{\pi}{4} D_{KA} \cdot Kn + D_{KA} \cdot Kn^2\right]} , \qquad (16)$$

in which $D_{KA} = \frac{2a\bar{v}}{3}$.

The data as plotted clearly show the asymptotic behavior for the continuum and Knudsen regimes with a well resolved transition between. We may observe a mid-transition point occuring at Kn ≈ 0.2. The Wakao model behaves well in the continuum regime but predicts permeabilities which are a little too large in the Knudsen flow regime. Transition occurs more abruptly for the experimental results than for Wakao's prediction, suggesting on physical grounds that a sudden freeze model may be found useful.

In these figures we have also plotted the permeability, k, versus Kn for each of the samples. The transition region is again approximately centered about Kn = 0.2. It is evident that in the Knudsen regime flows experience a much larger permeability than those in the continuum regime.

That does not mean, however, that the greatest impedance to flow is necessarily experienced in the continuum regime. The measure of local impedance may be considered to be proportional to the pressure gradient per unit of mass flowing, which we may represent by the quantity $\frac{\Delta p}{p_o \dot{\forall}_o}$ except for a factor of proportionality. This quantity is shown as a function of Kn in Figures 10, 11 and 12. We note in each instance that the normalized pressure gradient rises in approximately linear fashion over the region where the permeability is essentially constant. Thus we may show from Eq. 8 that $\Delta p/\Delta x \sim Kn \sim 1/p$ for k=const. and we find this prediction confirmed

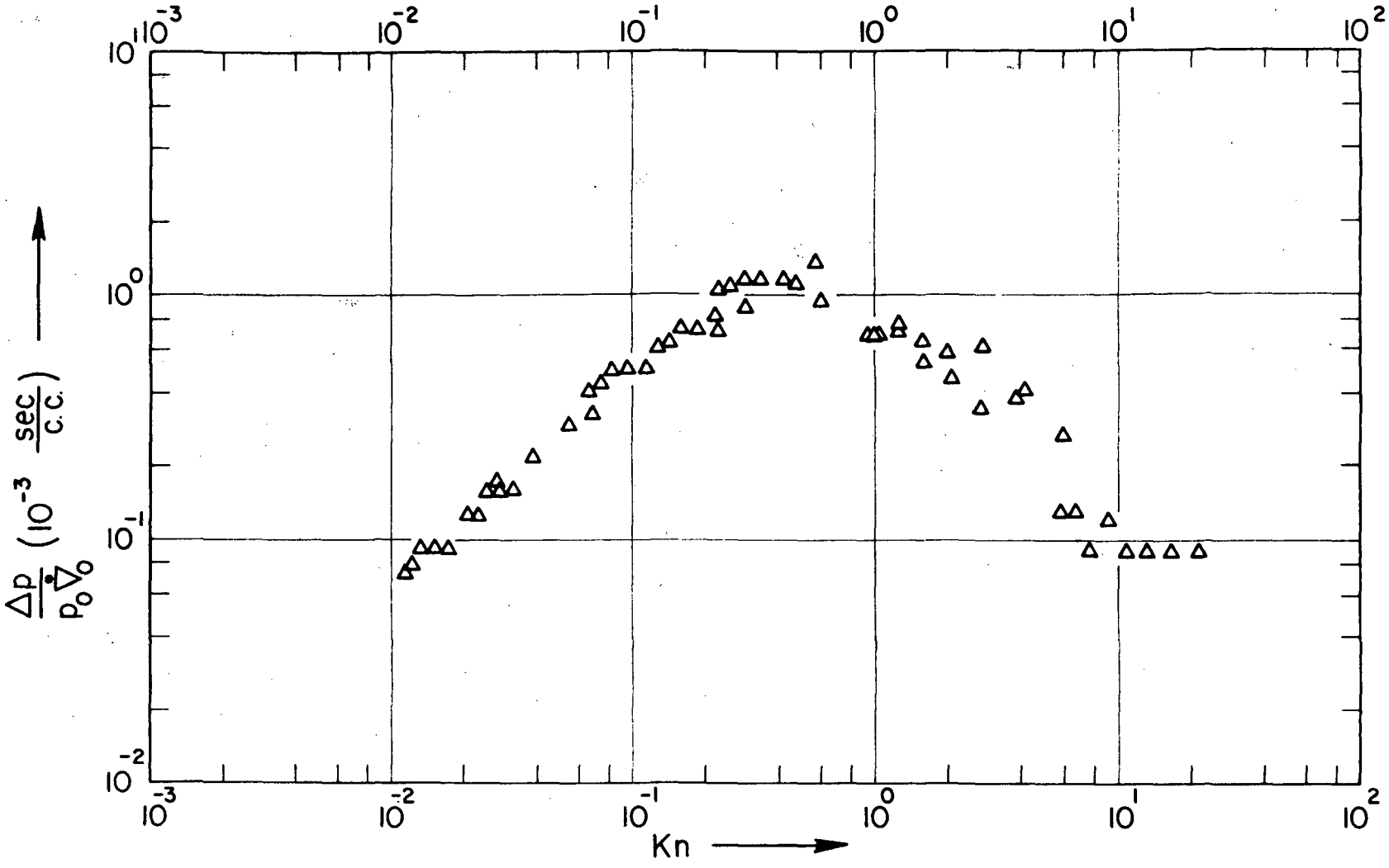

FIG. 10 MODIFIED PRESSURE GRADIENT $\frac{\Delta p}{p_o \dot{\nabla}_o}$ VS Kn FOR 3mm SINTERED GLASS BEAD SPECIMEN

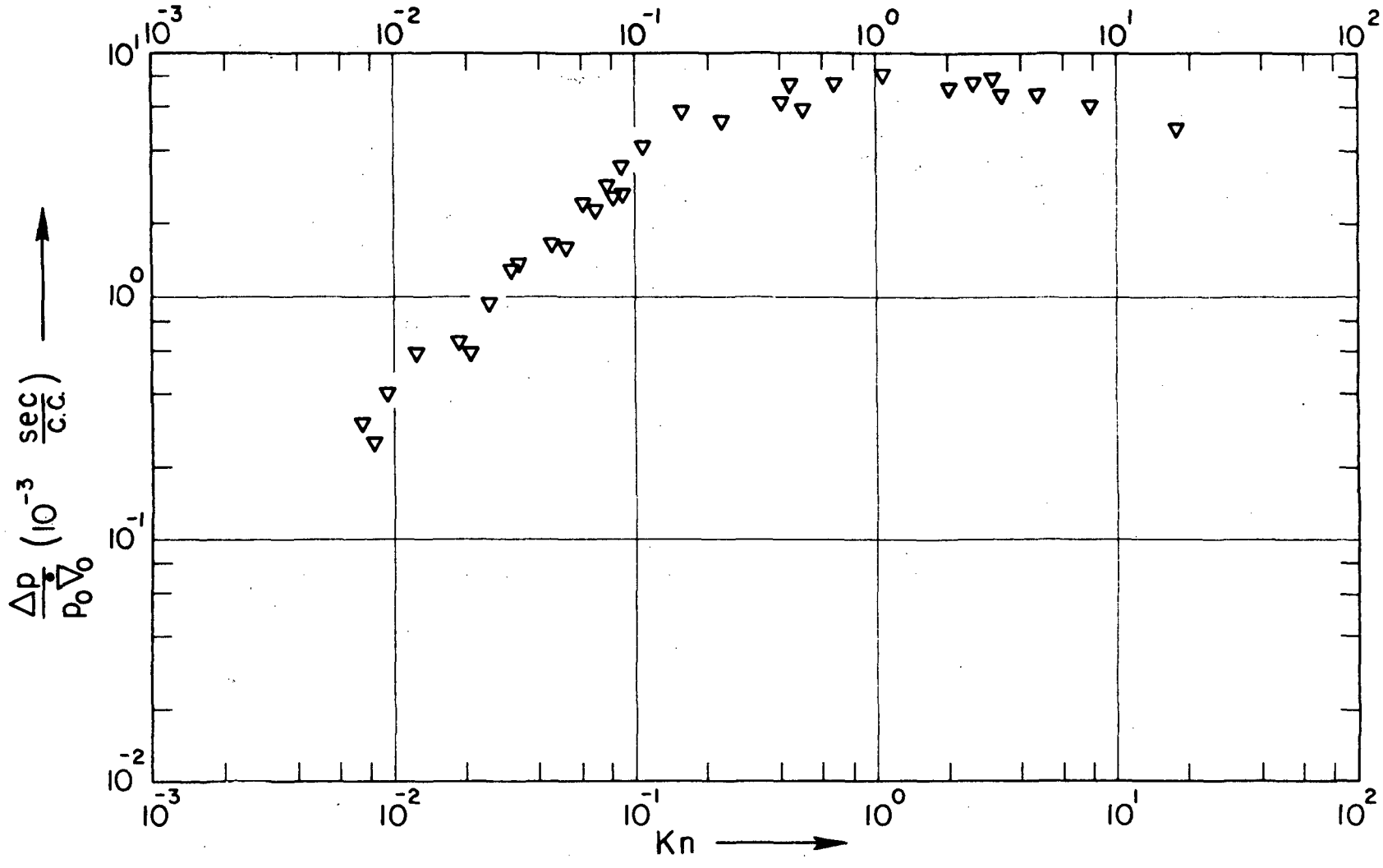

FIG. 11 MODIFIED PRESSURE GRADIENT $\frac{\Delta p}{p_o \dot{\nabla}_o}$ VS Kn FOR 3mm SINTERED GLASS BEAD SPECIMEN

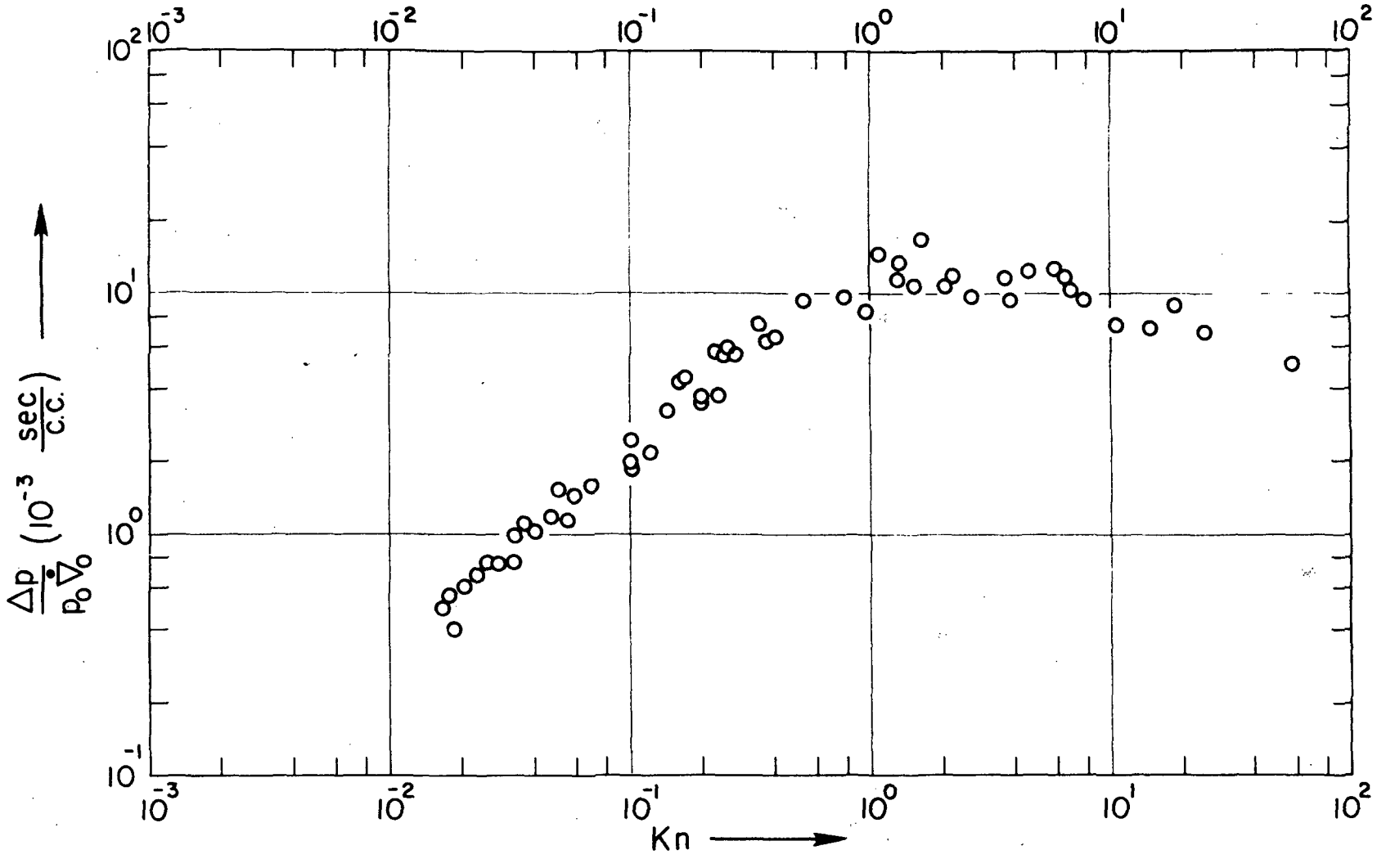

FIG. 12 MODIFIED PRESSURE GRADIENT $\frac{\Delta p}{p_0 \dot{\nabla}_0}$ VS Kn FOR SAND STONE SPECIMEN

by the observations. In the next section of these plots, from Kn $\approx$ 0.3 the flow has entered the transition regime and the permeability (Figures 7, 8, 9) is now found to undergo a steep rise. From this point on, the behavior of the pressure gradient is determined by a competition between the tendancy for that quantity to rise as a result of increasing rarefaction and its need to decrease as a result of the swiftly increasing permeability. The net effect produces a maximum in $\Delta p/\Delta x$ for Kn $\approx$ 0.4 to 1.0 followed by a decrease which is rather large for the 3mm bead specimen but rather small for the 4mm bead specimen and the sandstone. This maximum bears a strong qualitative relationship with the minima in Q observed for transition flows in several previous studies.

It is interesting to note the very substantial similarity between the latter two materials in this regard. One may conjecture that these materials are in fact quite similar in respect to some relevant shape factor which has not been considered in our analysis but which is of particular importance in Knudsen flows. We identify this point as one for further study.

The total impedance to flow experienced in any particular regime is given by the integral of the pressure gradient over the length of specimen in that regime. Accordingly in Figures 13 and 14 we have shown the variation in Kn over the length of the specimen for typical reference flow conditions. The concept of reduced length has been applied in the construction of these plots and the reference condition in each case has been chosen to produce continuum flows in the initial portions of the samples.

In Figure 13 the Knudsen number for the 3mm bead specimen is plotted as a function of its physical length, arbitrarily normalized to 8 units. We see a smooth curve, increasing evermore rapidly in slope as the downstream end of the sample is approached. Plots for the other specimens

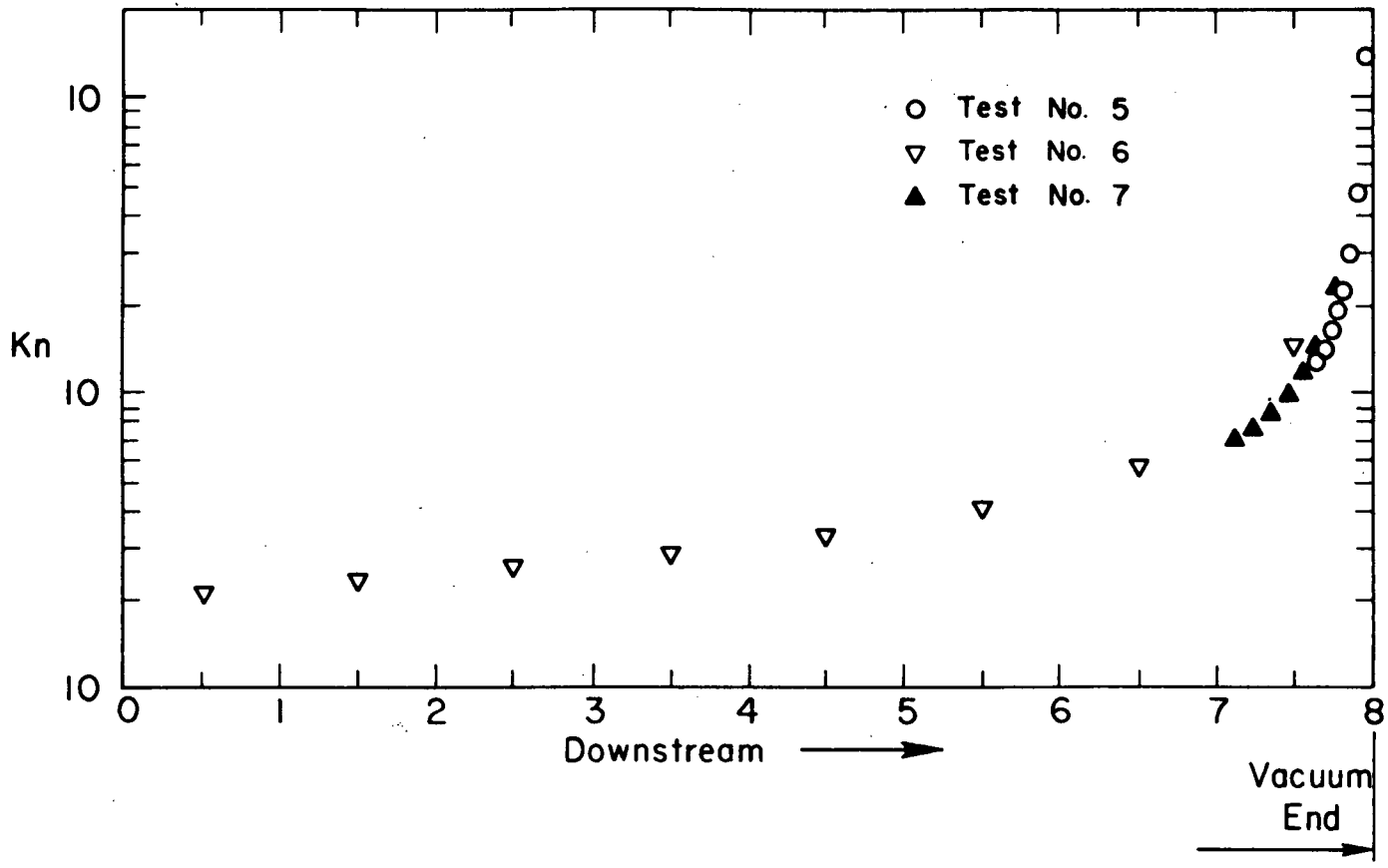

FIG. 13 KNUDSEN NUMBER VARIATION OVER THE LENGTH OF THE POROUS MEDIUM SPECIMEN MADE OF 3mm SINTERED GLASS BEADS

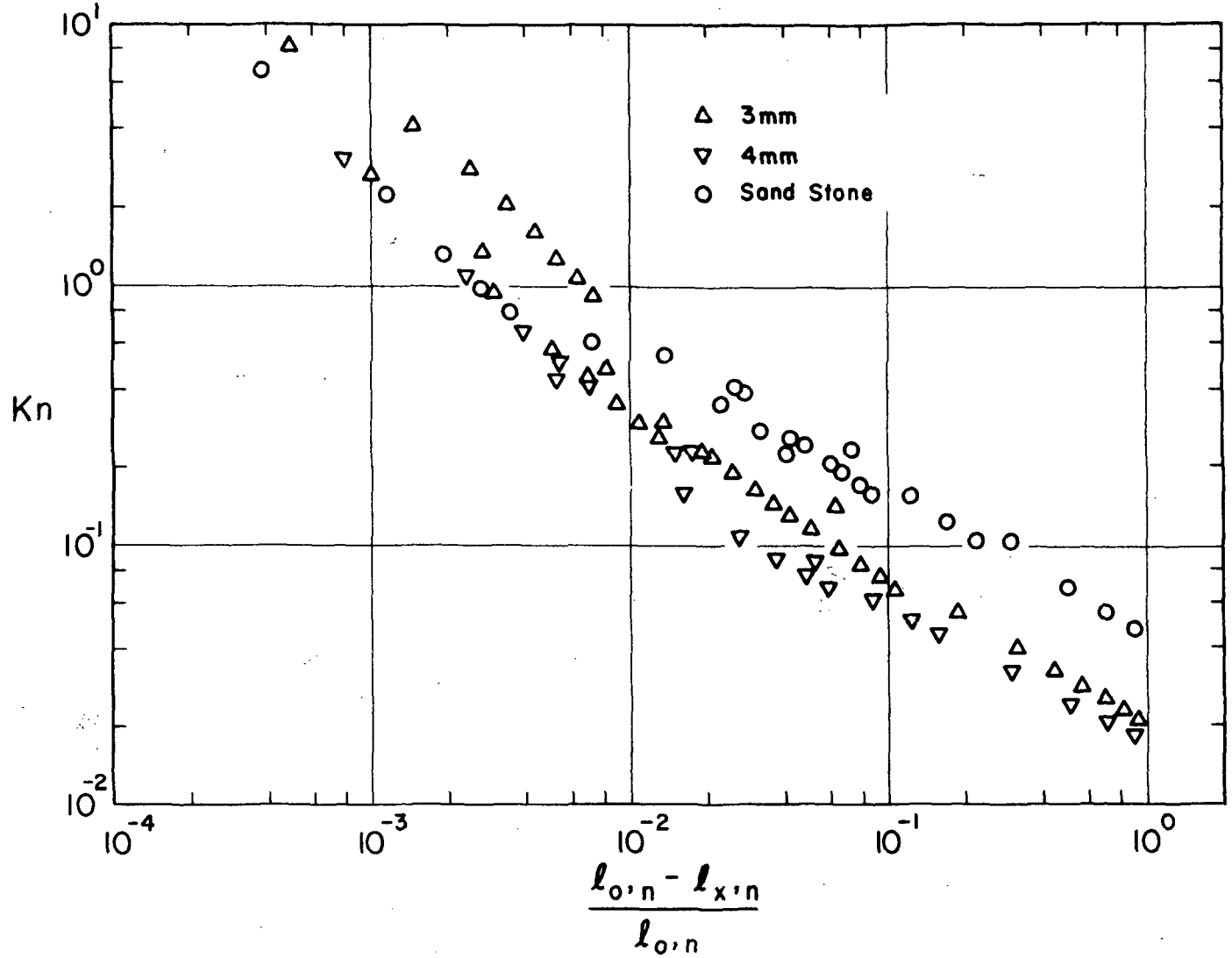

FIG. 14 KNUDSEN NUMBER VS FRACTION OF REMAINING LENGTH THROUGH SPECIMEN

(not included in this report) show very similar behavior. Typically the initial value of the Knudsen number is of the order of 10^{-2}, and mid transition at Kn $\simeq$ 0.2 occurs within 2% to 7% of the total length from the downstream end. A representation which is more sensitive to behavior at large Knudsen numbers, Figure 14, shows Kn as a function of the ratio of the length between a data point and the downstream end to the total length. Results for the three materials are shown on this plot. In the continuum regime, where $(\ell_{o,n} - \ell_{x,n})/\ell_{o,n} \geq 2 \times 10^{-2}$, the data points for the three materials lie along well defined curves which are more or less parallel. At smaller values of the length ratio the curves coalesce to a degree and assume a greater slope. The behavior is most consistently exhibited for the 4mm bead samples but the difficulties associated with the measurement of very small flow rates at the larger Knudsen numbers make a more precise description problematic. A comparison of Figure 14 with Figures 10, 11 and 12 leads however to the conclusion that in flows where the Knudsen number is initially as small as 10^{-2} the integrated pressure drop in the continuum regime dominates. It is evident at the same time that the relative pressure drop between the limiting regimes is determined by the initial Knudsen number as well as by the $\Delta p/\Delta x$ behavior discussed in the foregoing.

We return to the question of the value of the sudden freeze analysis given in the section on theory. From Figure 13 it would appear that the Knudsen number variation over the entire sample is continuous although more pronounced over the final 10 to 15 percent of the sample. Thus the abrupt upturn of the Knudsen number required for consistency with the sudden freeze analysis is not present. While the analysis would predict the ratio of length up to the freezing surface to that beyond, $\frac{X_1 - X_{exit}}{X_0 - X_1}$, to be of the

order of 10^{-4}, the point of mid-transition in the variation of Knudsen number would actually appear at a ratio of about 10^{-2} or larger. We must conclude that the physical behavior is not well described in such simple terms.

In the final plot, Figure 15, we have shown a comparison of the behavior of F(Kn) as a function of Kn for the three kinds of material. It is seen that the dimensionless function succeeds quite well in scaling the behavior for the continuum regime but that there is somewhat poorer agreement for the Knudsen regime. As we have suggested at an earlier point it is possible that some resolution of the observed differences might be made through an analysis which introduces a pore shape factor. This may be found to be equivalent to the introduction of a second Knudsen number.

CONCLUSIONS

The present study has demonstrated the applicability of the concept of local similarity to flows of gases in porous media in which the flow may undergo transition from the continuum to the Knudsen regimes. The reduction of data herein which has been based on this concept shows an entirely acceptable degree of internal consistency throughout the range of flow regimes. The same length parameter, the mean pore diameter, is used throughout, and this is derived from continuum flow measurements. The formulation is more successful than the interpolative Wakao formula but fails to account exactly for behavior in the Knudsen regime.

The experimental method has been shown to have promise for the study of the details of transition flows. It has been shown that flow behavior in synthetic specimens follows the same general patterns as that in one kind of natural material. It appears reasonable to suggest that study of

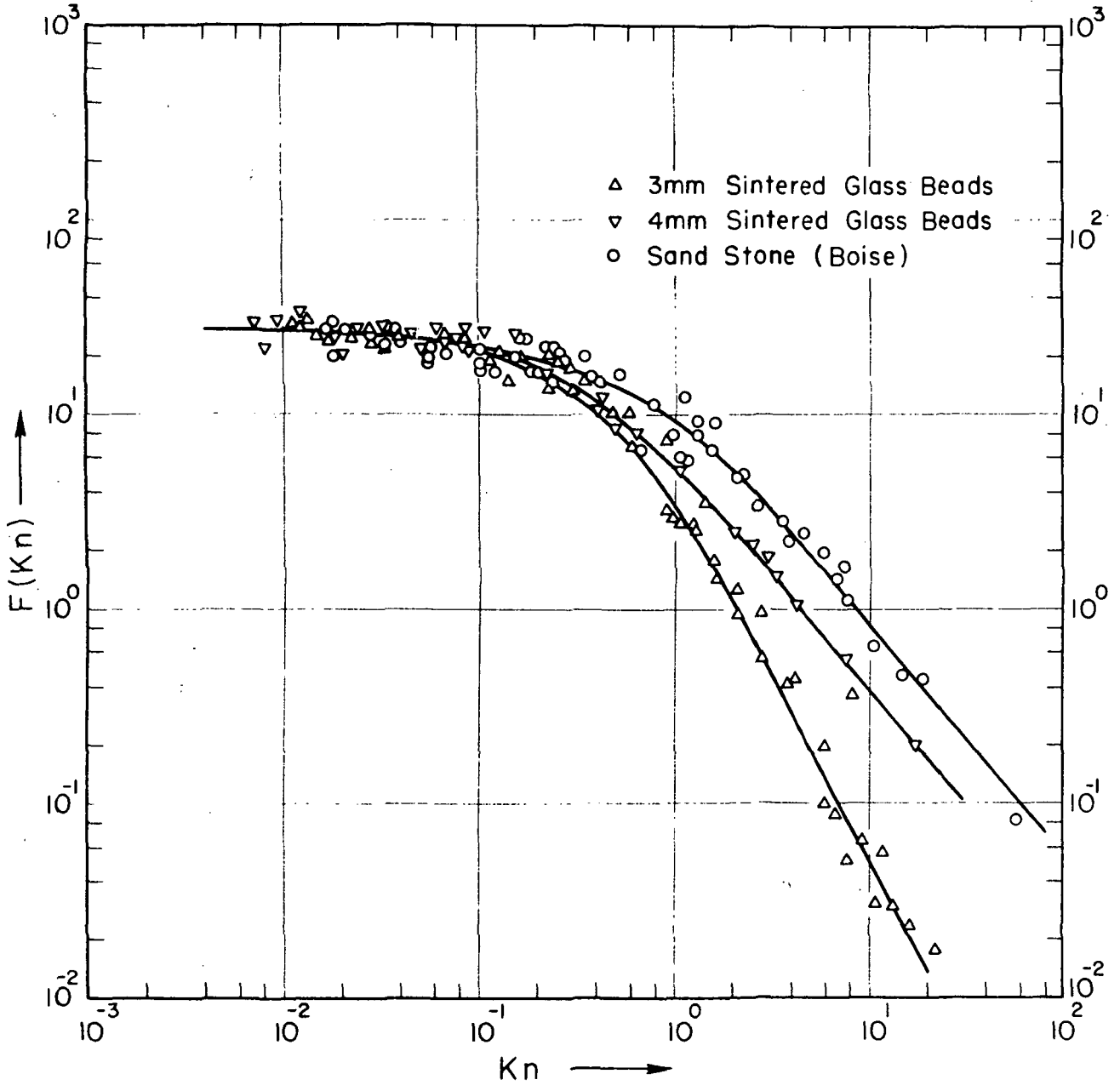

FIG. 15 F(Kn) VS Kn

additional forms of synthetic materials could lead to more detailed understanding of configuration effects in natural materials. The concept of sample segmentation, employed for the first time in these studies, has been demonstrated to have merit both through the general consistency of all the reduced data and particularly through the internal consistency of the plots of Knudsen number dependence on length, Figures 13 and 14.

It would appear that development specifically directed to a lunar permeability probe could now be undertaken with some confidence. From the present studies we learn that flow in the continuum regime will be dominant for one dimensional flows provided the entrance Knudsen number is sufficiently small, i.e., $Kn < 10^{-2}$. Practical consideration in a particular range of permeabilities may preclude the high entrance pressures appropriate in some cases in which event interpretations must take cognizance of flows initially in the rarefied regimes. Since the local similarity assumptions would appear to be adequately verified, techniques for interpreting pressure distributions determined from probe observation in terms of area fraction and pore diameter already discussed in previous reports (see Ref. 13 and Appendix B) will doubtless prove satisfactory.

It would appear from a consideration of our laboratory experience that the measurement of pressure distribution involving two or more points of observation will require sophisticated handling of the mechanical design of pressure seals. It is suggested that rock samples will probably require small bore holes for pressure instrumentation and that the development of a practicable probe system might follow this approach.

REFERENCES

1. Carman, P. C., Flow of Gases Through Porous Media, Academic Press, New York (1956).

2. Cercignani, Carlo and F. Sernagiotto, "Cylindrical Poiseuille Flow of a Rarefied Gas," Phys Fluid 9 40 (1966).

3. Evans, R. B., III, G. M. Watson and E. A. Mason, "Gaseous Diffusion in Porous Media at Uniform Presures," Jour Chem Phys 35, 2076 (1961).

4. Huang, J. H. and T. L. Ramsey, "Fluid Flow in Porous Media - Diffusion and Flow of Nitrogen in Natural Rocks," Jour Geophysical Res 73, 7085 (1968).

5. Hurlbut, F. C. et al., "Fluid Conductivity of Lunar Surface Materials," Final Report, Vol. IV of IV (Lunar Surface Engineering Properties Experiment Definition), SSL, Series 11, Issue 51, U. C. Berkeley, July 1971.

6. Lund, L. M. and A. S. Berman, "Flow and Self-Diffusion of Gases in Capillaries, Part I," J. A. P. 37, 2489 (1966).

7. Mason, E. A., A. P. Malinauskas and R. B. Evans, "Flow and Diffusion of Gases in Porous Media," Jour Chem Phys 46, 3199 (1967).

8. Mitchell, J. K. et al., "Lunar Surface Engineering Properties Experiment Definition," First Quarterly Report, SSL, Series 9, Issue 62, U. C. Berkeley, Oct. 1968.

9. Mitchell, J. K. et al., "Material Studies Related to Lunar Surface Exploration," Final Report, Vol. IV of IV, SSL, U. C. Berkeley, Nov. 1969.

10. Raghuraman, P., "Kinetic Theory Analysis of Rarefied Gas Flow Through Finite Length Slots," College of Engineering, U. C. Berkeley Report No. FM-72-1, Feb. 1972.

11. Sreekanth, A. K., "Slip Flow Through Long Circular Tubes," Proceedings of the 6th Rarefied Gas Dynamics Symposim L. Trilling, Ed., Academic Press (1969).

12. Wakao, N., S. Otani and J. M. Smith, "Significance of Pressure Gradients in Porous Materials: Part 1 Diffusion and Flow in Fine Capillaries," A. I. Che. E. Jour 11 435 (1965).

13. Witherspoon, P. A. and D. R. Willis, "Fluid Conductivity of Lunar Surface Materials," Final Report, Vol. IV of IV. Lunar Surface Eng. Properties SSL Series 11, Issue 13, Jan. 1970.

14. Zhdanov, V., Yu. Kagan and A. Sazykin, "Effect of Viscous Transfer of Momentum of Diffusion of a Gas Mixture," JETP 15 596 (1962).

NOMENCLATURE

a	Average pore radius, cm.
A	Cross sectional area of specimen, cm^2
c	Conductivity, defined Eq. 1
$\tilde{c}(p)$	Generalized conductivity, defined Eq. 3
f	Effective area fraction
$F(Kn)$	Dimensionless function, defined Eq. 4
k	Permeability, cm^2
Kn	Knudsen number, $Kn = \frac{\lambda}{2a}$
L	Characteristic length
$\ell_{1,2}$	Length of sample between coordinates x_1, x_2
p	Pressure, torr or microns Hg, as noted
$\bar{p}$	Arithmetic mean pressure
pc	Gas inlet pressure
Δp	Pressure difference
Q	Mass flow rate gm/sec
R	Gas constant, for N_2 $R = 2.97 \times 10^6 \frac{erg}{gm\ ^\circ K}$
T	Temperature, °K
$\bar{V}$	Average flow speed, cm/sec
$\bar{v}$	Mean molecular speed cm/sec
$\dot{V}o$	Volumetric flow rate (cm^3/sec) at po
Δx	Thickness of a sample disk, cm
ρo	Gas density at po, gm/cm^3
ρ	Gas density at p
μ	Absolute viscosity, poise
λ	Molecular mean-free-path, cm

APPENDIX A

Permeability Test Data

Table II

3mm Sintered Glass Beads Specimen

Sample Designation	Downstream →	3-14	3-8	3-9	3-11	3-3	3-10	3-6	3-5	3-7
Test Condition	Item	Units	Data and Calculated Results							
1.										
p_o = 765 Torr	p	μ (microns)	24	21	18	16	13	11	9	7	5
$\dot{\nabla}_o$ = 2.94 x 10^{-2} c.c./sec	$\bar{p}$	μ	22.5	19.5	17.	14.5	12.	10.	8	6
	$\frac{\Delta p}{p_o \dot{\nabla}_o}$	10^{-3} sec/c.c.	0.13	0.13	0.09	0.12	0.09	0.09	0.09	0.09
T = 24.7°C										
μ = 1.77 x 10^{-2} centipoise	$\frac{\Delta p^2}{p_o \dot{\nabla}_o} \frac{fA}{\Delta x}$	10^{-3} dyne-sec.	25.1	21.7	12.6	16.1	8.92	7.49	5.93	4.47
	Kn		5.85	6.70	7.74	9.10	10.9	13.2	16.4	21.9
	k	10^{-2} cm^2	1.41	1.62	1.98	2.17	3.94	4.71	5.92	7.85
	F(Kn)	10^{-2}	10	8.65	5.02	6.41	3.06	2.98	2.36	1.78
2.										
p_o = 754 Torr	p	μ	145	120	91	71	54	41	27	17	6
$\dot{\nabla}_o$ = 5x10^{-2} c.c./sec.	$\bar{p}$	μ	133	106	81	62.5	47.5	34	22	11.5
	$\frac{\Delta p}{p_o \dot{\nabla}_o}$	10^{-4} sec/c.c.	6.64	7.20	5.30	4.51	3.45	3.72	2.65	2.92
T = 23.5°C										

Sample Designation	Downstream → 3-14		3-8	3-9	3-11	3-3	3-10	3-6	3-5	3-7
Test Condition	Item	Units	Data and Calculated Results							
2. $\mu = 1.766 \times 10^{-2}$ centipoise	$\frac{\Delta p^2}{p_o \dot{\nabla}_o} \frac{fA}{\Delta x}$	10^{-2} dyne-sec.	73.4	67.7	35.9	23.5	13.7	10.5	4.89	1.40
	Kn		0.99	1.24	1.62	2.10	2.76	3.85	5.96	11.4
	k	10^{-4} cm^2	4.77	5.20	9.75	14.9	25.6	33.3	71.7	250
	F(Kn)	10^{-2}	294	272	144	94	54.9	42.0	19.6	5.61
3. p_o = 765 Torr	p	μ	154	134	114	92	73	56	38	26 6
$\dot{\nabla}_o = 3.84 \times 10^{-2}$ c.c./sec.	$\bar{p}$	μ	144	124	103	82.5	64.5	47	32	16
	$\frac{\Delta p}{p_o \dot{\nabla}_o}$	10^{-4} sec/c.c.	6.80	6.80	7.50	6.50	5.80	6.10	4.10	6.80
T = 24.9°C										
$\mu = 1.772 \times 10^{-2}$ centipoise	$\frac{\Delta p^2}{p_o \dot{\nabla}_o} \frac{fA}{\Delta x}$	10^{-2} dyne-sec.	81.6	70.9	64.6	44.7	31.1	24.0	10.9	9.11
	Kn		0.918	1.06	1.28	1.60	2.04	2.80	4.13	8.22
	k	10^{-4} cm^2	4.30	4.99	5.48	7.90	11.3	14.6	32.2	38.8
	F(Kn)		3.25	2.82	2.59	1.78	1.24	0.956	0.435	0.363

Sample Designation	Downstream → 3-14	3-8	3-9	3-11	3-3	3-10	3-6	3-5	3-7
Test Condition	Item	Units	Data and Calculated Results						
4.									
po = 783 Torr	p	μ	610	547	482	412	342	272	191	94	7
$\dot{\forall}o$ = 7.7 x10^{-2} c.c./sec.	$\bar{p}$	μ	578	515	448	377	307	232	142	50	
T = 25.3°C	$\frac{\Delta p}{po\dot{\forall}o}$	10^{-3} sec/c.c.	1.05	1.07	1.16	1.17	1.16	1.35	1.61	1.44	
μ = 1.772 x10^{-2} centipoise	$\frac{\Delta p^2}{po\dot{\forall}o} \frac{fA}{\Delta x}$	dyne-sec.	5.06	4.59	4.35	3.70	2.98	2.59	1.92	61.0	
	Kn	10^{-1}	2.27	2.55	2.94	3.49	4.29	5.67	9.28	26.3	
	k	10^{-5} cm^2	6.96	7.68	8.12	9.55	11.8	13.6	18.4	57.6	
	F(Kn)		20.2	18.3	17.3	14.7	11.9	10.3	.65	2.43	
5.									
po = 783 Torr	p	μ	1085	983	877	756	638	518	370	188	9.1
$\dot{\forall}o$ = 2.12 x10^{-1} c.c./sec.	$\bar{p}$	μ	1034	930	817	697	578	444	279	98.5	
T = 25.3°C	$\frac{\Delta p}{po\dot{\forall}o}$	10^{-3} sec/c.c.	0.61	0.64	0.73	0.72	0.72	0.89	1.10	1.08	
μ = 1.772 x10^{-2} centipoise	$\frac{\Delta p^2}{po\dot{\forall}o} \frac{fA}{\Delta x}$	dyne-sec.	5.30	4.97	4.97	4.18	3.46	3.32	2.56	0.886	
	Kn	10^{-1}	1.28	1.41	1.61	1.89	2.27	2.97	4.72	13.4	
	k	10^{-5} cm^2	6.64	7.10	7.10	8.46	10.2	10.6	13.7	39.9	
	F(Kn)		21.1	19.8	19.8	16.7	13.8	13.2	10.2	3.54	

Sample Designation	Downstream → 3-14		3-8	3-9	3-11	3-3	3-10	3-6	3-5	3-7
Test Condition	Item	Units	Data and Calculated Results							
6.										
po = 783 Torr	p	μ	6515	6039	5564	4966	4365	3764	2940	1828	33
$\dot{\nabla}o$ = 4.8 c.c./sec.	$\bar{p}$	$10^3\mu$	6.28	5.80	5.26	4.67	4.06	3.35	2.38	0.930	
T = 25.3°C	$\frac{\Delta p}{po\dot{\nabla}o}$	10^{-4} sec/c.c.	1.26	1.26	1.59	1.60	1.60	2.19	2.95	4.77	
μ = 1.772 x10^{-2} centipoise	$\frac{\Delta p^2}{po\dot{\nabla}o}\frac{fA}{\Delta x}$	dyne-sec.	6.64	6.14	6.96	6.23	5.43	6.14	5.89	3.71	
	Kn	10^{-2}	2.10	2.27	2.51	2.82	3.24	3.94	5.53	14.2	
	k	10^{-5} cm^2	5.31	5.75	5.04	5.65	6.48	5.75	5.98	9.48	
	F(Kn)	10	2.64	2.44	2.78	2.48	2.16	2.44	2.35	1.48	
7.										
po = 783 Torr	p	μ	2040	1866	1681	1470	1258	1046	772	418	12
$\dot{\nabla}o$ = 5.5 x10^{-1} c.c./sec.	$\bar{p}$	μ	1953	1774	1576	1364	1152	909	595	215	
T = 25.3°C	$\frac{\Delta p}{po\dot{\nabla}o}$	10^{-3} sec/c.c.	0.405	0.430	0.490	0.492	0.492	0.639	0.820	0.945	
μ = 1.772 x10^{-2} centipoise	$\frac{\Delta p^2}{po\dot{\nabla}o}\frac{fA}{\Delta x}$	dyne-sec.	6.58	6.39	6.46	5.61	4.73	4.85	4.08	1.70	
	Kn	10^{-2}	6.74	7.42	8.38	9.66	11.4	14.4	22.1	61.2	
	k	10^{-5} cm^2	5.34	5.54	5.43	6.28	7.44	7.28	8.62	20.7	
	F(Kn)	10	2.62	2.54	2.58	2.24	1.88	1.93	1.63	0.678	

Sample Designation	Downstream → 3-14		3-8	3-9	3-11	3-3	3-10	3-6	3-5	3-7
Test Condition	Item	Units	Data and Calculated Results							
8.										
po = 783 Torr	p	$10^3\mu$	12.06	11.22	10.32	9.27	8.22	7.17	5.72	3.75 0.065
T = 25.3°C	$\bar{p}$	$10^3\mu$	11.64	10.72	9.80	8.75	7.70	6.45	4.74	1.91
$\dot{\nabla}o$ = 14.6 c.c./sec.	$\frac{\Delta p}{po\dot{\nabla}o}$	10^{-5} sec/c.c.	7.30	7.90	9.2	9.20	9.20	12.7	17.3	32.3
μ= 1.772 x10^{-2} centipoise	$\frac{\Delta p^2}{po\dot{\nabla}o}\frac{fA}{\Delta x}$	dyne-sec.	7.22	7.09	7.53	6.71	5.93	6.84	6.84	5.14
	Kn	10^{-3}	1.13	1.23	1.34	1.51	1.71	2.04	2.78	6.90
	k	10^{-5} cm^2	4.91	4.96	4.68	5.23	5.93	5.13	5.13	6.86
	F(Kn)	10	2.88	2.82	3.00	2.68	2.36	2.72	2.72	2.05

Permeability Test Data

Table III

4mm Sintered Glass Beads Specimen

Sample Designation	Downstream → 4-1	4-9	4-5	4-4	4-8	4-11	4-3	4-2
Test Condition	Item	Units	Data and Calculated Results					
1.								
p_o = 760 Torr	p	μ	109	90	70	52	34	18	5
T = 25.5°C	$\bar{p}$	μ	100	80	61	43	26	11.5
$\dot{\nabla}_o$ = 3.45 x10^{-3} c.c./sec.	$\frac{\Delta p}{p_o \dot{\nabla}_o}$	10^{-3} sec/c.c.	7.25	7.64	6.86	6.86	6.10	4.96
μ = 1.774 x10^{-2} centipoise	$\frac{\Delta p^2}{p_o \dot{\nabla}_o} \frac{fA}{\Delta x}$	10^{-1} dyne-sec.	14.9	12.6	8.66	6.09	3.28	1.17
	Kn		2.02	2.53	3.31	4.70	7.78	17.6
	k	10^{-4} cm^2	4.55	5.40	7.85	12.2	20.7	58.0
	F(Kn)		2.54	2.15	1.48	1.04	0.56	0.20
2.								
p_o = 760 Torr	p	μ	540	447	359	246	125	6
T = 25.6°C	$\bar{p}$	μ	494	403	303	185.5	65.6
$\dot{\nabla}_o$ = 1.96 x10^{-2} c.c./sec.	$\frac{\Delta p}{p_o \dot{\nabla}_o}$	10^{-3} sec/c.c.	6.24	5.91	7.59	8.12	7.99
μ = 1.774 x10^{-2} centipoise	$\frac{\Delta p^2}{p_o \dot{\nabla}_o} \frac{fA}{\Delta x}$	dyne-sec.	6.37	4.90	4.75	3.10	1.08

Sample Designation	Downstream → 4-1		4-9	4-5	4-4	4-8	4-11	4-3	4-2
Test Condition	Item	Units	Data and Calculated Results						
2.									
	Kn	10^{-1}			4.09	5.00	6.67	10.9	30.9
	k	10^{-4} cm^2			1.07	1.39	1.44	2.19	6.28
	F(Kn)				10.9	8.36	8.10	5.29	1.84
3.									
po = 777.6 Torr	p	μ	3080	2802	2454	2134	1628	920	8
$\dot{\nabla}o$ = 1.57 $x10^{-1}$ c.c./sec.	$\bar{p}$	μ	2941	2628	2294	1881	1274	464	
T = 25.8°C	$\frac{\Delta p}{po\dot{\nabla}o}$	10^{-3} sec/c.c.	2.28	2.85	2.62	4.15	5.80	7.48	
μ = 1.775 $x10^{-2}$ centipoise	$\frac{\Delta p^2}{po\dot{\nabla}o} \frac{fA}{\Delta x}$	10 dyne-sec.	1.38	1.54	1.24	1.60	1.52	0.716	
	Kn	10^{-2}	6.86	7.66	8.84	10.8	15.9	43.6	
	k	10^{-5} cm^2	4.92	4.42	5.5	4.23	4.45	9.5	
	F(Kn)	10	2.36	2.63	2.12	2.73	2.60	1.22	
4.									
po = 777.6 Torr	p	μ	4742	4195	3674	2874	1750	13	
T = 26.0°C	$\bar{p}$	μ		4469	3935	3274	2312	882	
$\dot{\nabla}o$ = 4.25 $x10^{-1}$ c.c./sec.	$\frac{\Delta p}{po\dot{\nabla}o}$	10^{-3} sec/c.c.		1.66	1.58	2.42	3.40	5.26	
μ = 1.777 $x10^{-2}$ centipoise	$\frac{\Delta p^2}{po\dot{\nabla}o} \frac{fA}{\Delta x}$	10 dyne-sec.		1.52	1.28	1.64	1.63	0.954	

Sample Designation	Downstream → 4-1	4-9	4-5	4-4	4-8	4-11	4-3	4-2
Test Condition	Item	Units	Data and Calculated Results					
4.								
	Kn	10^{-2}		4.52	5.14	6.18	8.78	23.0
	k	10^{-5} cm^2		4.47	5.35	4.16	4.18	7.15
	F(Kn)	10		2.59	2.18	2.80	2.78	1.62
5.								
po = 777.6 Torr	p	10^3 μ	11.59	10.35	9.45	7.45	4.93	0.024
T = 26.1°C	$\bar{p}$	10^3 μ		10.97	9.80	8.35	6.19	2.48
$\dot{\nabla}o$ = 2.44 c.c./sec.	$\frac{\Delta p}{po\dot{\nabla}o}$	10^{-3} sec/c.c.		0.654	0.585	0.943	1.33	2.59
μ = 1.777 x10^{-2} centipoise	$\frac{\Delta p^2}{po\dot{\nabla}o}\frac{fA}{\Delta x}$	10 dyne-sec.		1.47	1.18	1.62	1.69	1.32
	Kn	10^{-2}		1.85	2.06	2.42	3.28	8.16
	k	10^{-5} cm^2		4.62	5.75	4.21	4.03	5.15
	F(Kn)	10		2.50	2.01	2.76	2.88	2.25
6.								
po = 777.6 Torr	p	10^3 μ	29.03	25.95	23.41	19.32	13.28	0.059
T = 26.1°C	$\bar{p}$	10^3 μ		27.50	24.68	21.36	16.30	6.67
$\dot{\nabla}o$ = 13.1 c.c./sec.	$\frac{\Delta p}{po\dot{\nabla}o}$	10^{-3} sec/c.c.		0.302	0.25	0.40	0.59	1.30
μ = 1.777 x10^{-2} centipoise	$\frac{\Delta p^2}{po\dot{\nabla}o}\frac{fA}{\Delta x}$	10 dyne-sec.		1.71	1.27	1.76	1.99	1.78

Sample Designation	Downstream → 4-1		4-9	4-5	4-4	4-8	4-11	4-3	4-2
Test Condition	Item	Units	Data and Calculated Results						
6.									
	Kn	10^{-3}			7.35	8.22	9.46	12.4	30.4
	k	10^{-5} cm^2			3.98	5.40	3.86	3.42	3.82
	F(Kn)	10			2.92	2.16	3.00	3.39	3.04

Permeability Test Data

Table IV

Sand Stone Specimen

Sample Designation	Downstream → 5-6	5-7	5-4	5-5	5-10	5-1	5-14	5-12	5-2
Test Condition	Item	Units	Data and Calculated Results							
1.										
po = 755 Torr	p	μ	200	174	140	105	79	58	38	20	5.5
T = 24°C	$\bar{p}$	μ	187	157	122	92	68	48	29	12.5	
$\dot{\nabla}o = 3.68 \times 10^{-3}$ c.c./sec.	$\frac{\Delta p}{po\dot{\nabla}o}$	10^{-3} sec/c.c.	9.35	12.2	12.4	9.35	7.37	7.20	6.83	5.04	
$\mu = 1.7771 \times 10^{-2}$ centipoise	$\frac{\Delta p^2}{po\dot{\nabla}o} \frac{fA}{\Delta x}$	dyne-sec.	16.7	18.2	14.5	8.22	4.83	3.34	0.875	0.603	
	Kn		3.87	4.60	5.89	7.80	10.5	14.9	24.8	57.6	
	k	10^{-5} cm^2	3.16	2.89	3.62	6.42	10.9	15.8	27.8	87.5	
	F(Kn)		2.26	2.46	1.96	1.11	0.652	0.451	0.118	0.0815	
2.										
po = 755 Torr	p	μ	700	595	500	385	307	237	153	70	6
T = 24.8°C	$\bar{p}$	μ	648	548	442	346	272	195	111.5	38	
$\dot{\nabla}o = 9.52 \times 10^{-3}$ c.c./sec.	$\frac{\Delta p}{po\dot{\nabla}o}$	10^{-3} sec/c.c.	14.6	13.2	16.5	10.85	9.74	11.7	11.5	8.90	
$\mu = 1.772 \times 10^{-2}$ centipoise	$\frac{\Delta p^2}{po\dot{\nabla}o} \frac{fA}{\Delta x}$	10 dyne-sec.	9.01	6.91	6.78	3.59	2.53	2.15	1.23	0.323	

Sample Designation	Downstream→ 5-6		5-7	5-4	5-5	5-10	5-1	5-14	5-12	5-2
Test Condition	Item	Units	Data and Calculated Results							
	Kn		1.10	1.31	1.63	2.08	2.63	3.68	6.45	18.9
	k	10^{-6} cm^2	5.83	7.59	7.77	14.7	20.8	24.4	42.7	163
	F(Kn)		12.2	9.33	9.15	4.85	3.42	2.90	1.66	0.436
3.										
po = 755 Torr	p	μ	1017	828	664	441	208	5.5		
T = 25.1°C	$\bar{p}$	μ	922	746	552	324	107			
$\dot{\nabla}o$ = 9.52 x10^{-3} c.c./sec.	$\frac{\Delta p}{po\dot{\nabla}o}$	10^{-3} sec/c.c.	9.52	8.26	11.23	11.7	10.2			
μ = 1.772 x10^{-2} centipoise	$\frac{\Delta p^2}{po\dot{\nabla}o} \frac{fA}{\Delta x}$	10 dyne-sec.	8.36	5.88	5.93	3.63	1.04			
	Kn	10^{-1}	7.80	9.67	13.0	22.2	68.0			
	k	10^{-6} cm^2	6.28	8.95	8.88	14.5	50.8			
	F(Kn)		11.3	7.94	8.00	4.90	1.41			
4.										
po = 772.6 Torr	p	μ	3330	2852	2377	1740	940	7		
$\dot{\nabla}o$ = 1.12 x10^{-1} c.c./sec.	$\bar{p}$	μ	3091	2614	2058	1340	474			
	$\frac{\Delta p}{po\dot{\nabla}o}$	10^{-3} sec/c.c.	5.53	5.49	7.36	9.25	10.8			
T = 25.3°C										
μ = 1.772 x10^{-2} centipoise	$\frac{\Delta p^2}{po\dot{\nabla}o} \frac{fA}{\Delta x}$	10^{-2} dyne-sec.	1.63	1.38	1.45	1.18	48.8			

Sample Designation	Downstream → 5-6	5-7	5-4	5-5	5-10	5-1	5-14	5-12	5-2
Test Condition	Item	Units	Data and Calculated Results						
4.									
	Kn	10^{-1}			2.33	2.75	3.50	5.37	15.2
	k	10^{-6} cm^2			3.23	3.84	3.64	4.45	10.8
	F(Kn)	10			2.20	1.86	1.96	1.59	0.66
5.									
po = 772.6 Torr	p	μ	4587	3851	3254	2298	1227	8	
T = 25.3°C	$\bar{p}$	μ			4219	3553	2776	1763	618
$\dot{\nabla}o$ = 0.214 c.c./sec.	$\frac{\Delta p}{po\dot{\nabla}o}$	10^{-3} sec/c.c.			4.46	3.62	5.80	6.50	7.39
μ = 1.772 $x10^{-2}$ centipoise	$\frac{\Delta p^2}{po\dot{\nabla}o}\frac{fA}{\Delta x}$	10^2 dyne-sec.			1.80	1.23	1.54	1.09	0.435
	Kn	10^{-1}			1.31	2.02	2.59	4.08	11.6
	k	10^{-6} cm^2			2.92	4.28	3.42	4.80	12.1
	F(Kn)	10			2.43	1.66	2.08	1.47	0.587
6.									
po = 767.5 Torr	p	μ	4850	4070	3440	2440	1310	8	
T = 24.3°C	$\bar{p}$	μ			4460	3760	2940	1880	660
$\dot{\nabla}o$ = 0.235 c.c./sec.	$\frac{\Delta p}{po\dot{\nabla}o}$	10^{-3} sec/c.c.			4.32	3.49	5.54	6.26	7.22
μ = 1.770 $x10^{-2}$ centipoise	$\frac{\Delta p^2}{po\dot{\nabla}o}\frac{fA}{\Delta x}$	10^2 dyne-sec.			1.84	1.25	1.56	1.13	0.451

Sample Designation	Downstream → 5-6	5-7	5-4	5-5	5-10	5-1	5-14	5-12	5-2
Test Condition	Item	Units	Data and Calculated Results						
6.									
	Kn	10^{-1}			1.61	1.90	2.44	3.82	10.9
	k	10^{-6} cm^2			2.85	4.20	3.39	4.68	11.7
	F(Kn)	10			2.48	1.69	2.11	1.53	0.609
7.									
po = 772.6 Torr	p	μ	7524	6400	5412	3920	2184	12	
T = 25.3°C	$\bar{p}$	μ			6962	5906	4666	3052	1098
$\dot{\nabla}o$ = 0.595 c.c./sec.	$\frac{\Delta p}{po\dot{\nabla}o}$	10^{-3} sec/c.c.			2.44	2.15	3.24	3.77	4.72
μ = 1.772 x10^{-2} centipoise	$\frac{\Delta p^2}{po\dot{\nabla}o}\frac{fA}{\Delta x}$	10^2 dyne-sec.			1.62	1.22	1.45	1.10	0.497
	Kn	10^{-1}			1.03	1.22	1.54	2.36	6.56
	k	10^{-6} cm^2			3.23	4.34	3.62	4.77	10.6
	F(Kn)	10^1			2.18	1.65	1.96	1.48	0.671
8.									
po = 772.6 Torr	p	μ	16,320	14,120	11,960	8,960	5,210	22	
T = 25.3°C	$\bar{p}$	$10^3\mu$			15.22	13.04	10.46	7.09	2.62
$\dot{\nabla}o$ = 2.44 c.c./sec.	$\frac{\Delta p}{po\dot{\nabla}o}$	10^{-3} sec/c.c.			1.17	1.15	1.59	1.99	2.76
μ = 1.772 x10^{-2} centipoise	$\frac{\Delta p^2}{po\dot{\nabla}o}\frac{fA}{\Delta x}$	10^2 dyne-sec.			1.70	1.43	1.59	1.35	0.691

Sample Designation	Downstream → 5-6	5-7	5-4	5-5	5-10	5-1	5-14	5-12	5-2
Test Condition	Item	Units			Data and Calculated Results				
8.									
	Kn	10^{-2}			4.73	5.52	6.86	10.2	27.5
	k	10^{-6} cm^2			3.10	3.68	3.30	3.91	7.66
	F(Kn)	10			2.30	1.93	2.15	1.82	0.933
9.									
po = 767.5 Torr	p	μ			16,450	14,200	11,980	8,980	5,230
T = 24.3°C	$\bar{p}$	$10^3\mu$			15.32	13.09	10.48	7.11	2.63
$\dot{\nabla}o$ = 2.6 c.c./sec.	$\frac{\Delta p}{po\dot{\nabla}o}$	10^{-3} sec/c.c.			1.125	1.11	1.5	1.88	2.60
μ = 1.770 x10^{-2} centipoise	$\frac{\Delta p^2}{po\dot{\nabla}o}\frac{fA}{\Delta x}$	10^2 dyne-sec.			1.65	1.39	1.50	1.27	0.655
	Kn	10^{-2}			4.68	5.49	6.86	10.1	27.3
	k	10^{-6} cm^2			3.19	3.80	3.50	4.14	8.04
	F(Kn)	10			2.23	1.88	2.02	1.31	0.885
10.									
po = 772.6 Torr	p	μ			27,450	23,950	20,360	15,620	9,080
T = 25.3°C	$\bar{p}$	$10^3\mu$			25.7	22.16	18.0	12.4	4.56
$\dot{\nabla}o$ = 6.0 c.c./sec.	$\frac{\Delta p}{po\dot{\nabla}o}$	10^{-3} sec/c.c.			0.754	0.774	1.02	1.41	1.95
μ = 1.772 x10^{-2} centipoise	$\frac{\Delta p^2}{po\dot{\nabla}o}\frac{fA}{\Delta x}$	10^2 dyne-sec.			1.86	1.64	1.75	1.66	0.849

Sample Designation	Downstream → 5-6	5-7	5-4	5-5	5-10	5-1	5-14	5-12	5-2
Test Condition	Item	Units	Data and Calculated Results						
10.									
	Kn	10^{-2}			2.80	3.24	4.0	5.80	15.8
	k	10^{-6} cm^2			2.85	3.21	3.01	3.16	6.19
	F(Kn)	10			2.51	2.22	2.36	2.24	1.15
11.									
po = 772.6 Torr	p	μ			45,900	40,100	35,430	27,630	15,970 65
T = 25.3°C	$\bar{p}$	$10^3\mu$			43.0	37.8	31.53	21.8	8.02
$\dot{\nabla}o$ = 15 c.c./sec.	$\frac{\Delta p}{po\dot{\nabla}o}$	10^{-3} sec/c.c.			0.50	0.403	0.672	1.00	1.37
μ = 1.772 $x10^{-2}$ centipoise	$\frac{\Delta p^2}{po\dot{\nabla}o}\frac{fA}{\Delta x}$	10^2 dyne-sec.			2.05	1.45	2.03	2.09	1.05
	Kn	10^{-2}			1.67	1.84	2.28	3.30	9.02
	k	10^{-6} cm^2			2.55	3.62	2.60	2.51	5.02
	F(Kn)	10			2.77	1.96	2.74	2.82	1.42
12.									
po = 767.5 Torr	p	μ			42,900	37,500	31,750	24,620	14,280 55
T = 25.0°C	$\bar{p}$	$10^3\mu$			40.2	34.62	28.18	19.45	7.17
$\dot{\nabla}o$ = 12.3 c.c./sec.	$\frac{\Delta p}{po\dot{\nabla}o}$	10^{-3} sec/c.c.			0.572	0.609	0.755	1.10	1.51
μ = 1.772 $x10^{-2}$ centipoise	$\frac{\Delta p^2}{po\dot{\nabla}o}\frac{fA}{\Delta x}$	10^2 dyne-sec.			2.20	2.02	2.04	2.04	1.03

Sample Designation		Downstream → 5-6	5-7	5-4	5-5	5-10	5-1	5-14	5-12	5-2
Test Condition	Item	Units	Data and Calculated Results							
12.										
	Kn	10^{-2}				1.79	2.08	2.55	3.70	10.1
	k	10^{-6} cm^2				2.40	2.62	2.58	2.58	5.11
	F(Kn)	10				2.97	2.73	2.76	2.76	1.39

APPENDIX B

Utilization of Permeability Probe Data for Determination of Area Fraction and Pore Diameter

The interpretation of pressures determined by probe measurements at various distances, r, from a gas source undertaken with the objective of determining the area fraction and pore diameter has been described in earlier reports of this series (Ref. 8 and 13). A brief account of the method proposed will be repeated here. Only one-dimensional flows will be discussed in this note but one can easily make the extension to two and three dimensional axi-symmetric flows.

Since the flow is one-dimensional we replace r by x. We also

$$\text{let } F(kn) = F_1(\zeta) \text{ where} \tag{1B}$$

$$\zeta \equiv \frac{1}{Kn} \tag{2B}$$

The foregoing substitution, which states that a function F of the Knudsen number is equivalent to a function F_1 of the inverse of the Knudsen number, is made for convenience and to bring the notation of this note into accord with the earlier work.

From Eq. 7 and the above definition we find that

$$F_1(\zeta) = \frac{f_\infty A}{(\rho_o \bar{v}_o)} \frac{L^2}{\mu} \frac{\rho}{RT} \frac{dp}{dx} \tag{3B}$$

also we may write, from Eq. (6)

$$\frac{1}{Kn} = \zeta = \frac{\bar{p}\bar{v}L}{2\mu RT} \tag{4B}$$

We now take the logarithms of Eq. (3B) and (4B) with the result that

$$\ell n\, \zeta = \ell n\, [p] + \ell n \left[\frac{\bar{v}L}{2\mu RT}\right] \tag{5B}$$

and

$$\ell n\ F_1(\zeta) = \ell n \left[p\frac{dp}{dx}\right] + \ell n \left[\frac{fAL^2}{\rho o \bar{V} o \mu RT}\right] \tag{6B}$$

The ratio of the derivatives of these expressions may be written

$$\frac{d\ \ell n F_1(\zeta)}{d\ \ell n\ \zeta} = \frac{d\ \ell n \left[p\ \frac{dp}{dx}\right]}{d\ \ell n\ [p]} \tag{7B}$$

It follows that the curves of $F_1(\zeta)$ vs ζ and $p\ \frac{dp}{dx}$ vs p, plotted on identical log-log scales, differ only in the positions of their respective origins of coordinates. Thus, measured values of $p\ \frac{dp}{dx}$ are plotted vs p on log-log paper, and $F_1(\zeta)$ vs ζ is plotted on identical paper. The two plots are adjusted until the data points lie on the known curve. The coordinates of the origin of the experimental plot relative to the universal curve clearly yield both f and L. The superposition of experimental data points and universal curve is illustrated in Figure B-1.

Since experimental error will influence the supposed relative positions of the two origins it should be evident the statistical reliability of determinations of f and L will depend upon that of the data points. Thus it appears probable that study of probe design and performance will show the desirability of obtaining several measurements per sample.

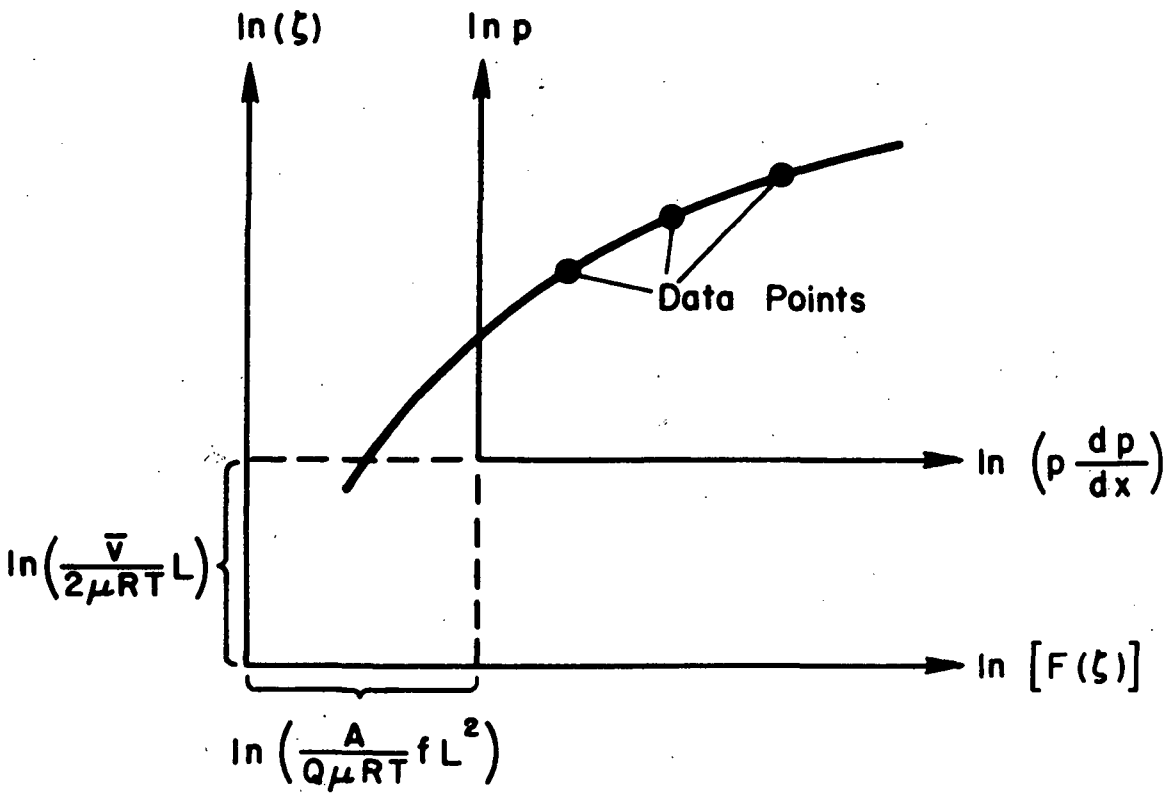

FIG. B-1 EXAMPLE OF MATCHING PROCEDURE IN DETERMINING PORE DIAMETER AND AREA FRACTION